**Atmospheric
Chemistry
and Physics**

Coupling of HO_x, NO_x and halogen chemistry in the antarctic boundary layer

W. J. Bloss[1], **M. Camredon**[1,*], **J. D. Lee**[2], **D. E. Heard**[3], **J. M. C. Plane**[3], **A. Saiz-Lopez**[4], **S. J.-B. Bauguitte**[5], **R. A. Salmon**[5], **and A. E. Jones**[5]

[1]School of Geography, Earth and Environmental Sciences, University of Birmingham, Edgbaston, Birmingham, B15 2TT, UK
[2]Department of Chemistry, University of York, Heslington, York YO10 5DD, UK
[3]School of Chemistry, University of Leeds, Leeds LS2 9JT, UK and National Centre for Atmospheric Science, School of Chemistry, University of Leeds, Leeds LS2 9JT, UK
[4]Laboratory for Atmospheric and Climate Science, Consejo Superior de Investigaciones Cientificas (CSIC), Toledo, Spain
[5]British Antarctic Survey, Natural Environment Research Council, High Cross, Madingley Road, Cambridge, CB3 0ET, UK
[*]now at: LISA, UMR CNRS/INSU 7583, Université Paris Est Créteil et Université Paris Diderot, Institut Pierre Simon Laplace, 94010 Créteil Cedex, France

Abstract. A modelling study of radical chemistry in the coastal Antarctic boundary layer, based upon observations performed in the course of the CHABLIS (Chemistry of the Antarctic Boundary Layer and the Interface with Snow) campaign at Halley Research Station in coastal Antarctica during the austral summer 2004/2005, is described: a detailed zero-dimensional photochemical box model was used, employing inorganic and organic reaction schemes drawn from the Master Chemical Mechanism, with additional halogen (iodine and bromine) reactions added. The model was constrained to observations of long-lived chemical species, measured photolysis frequencies and meteorological parameters, and the simulated levels of HO_x, NO_x and XO compared with those observed. The model was able to replicate the mean levels and diurnal variation in the halogen oxides IO and BrO, and to reproduce NO_x levels and speciation very well. The NO_x source term implemented compared well with that directly measured in the course of the CHABLIS experiments. The model systematically overestimated OH and HO_2 levels, likely a consequence of the combined effects of (a) estimated physical parameters and (b) uncertainties within the halogen, particularly iodine, chemical scheme. The principal sources of HO_x radicals were the photolysis and bromine-initiated oxidation of HCHO, together with $O(^1D) + H_2O$. The main sinks for HO_x were peroxy radical self- and cross-reactions, with the sum of all halogen-mediated HO_x loss processes accounting for 40% of the total sink. Reactions with the halogen monoxides dominated CH_3O_2-HO_2-OH interconversion, with associated local chemical ozone destruction in place of the ozone production which is associated with radical cycling driven by the analogous NO reactions. The analysis highlights the need for observations of physical parameters such as aerosol surface area and boundary layer structure to constrain such calculations, and the dependence of simulated radical levels and ozone loss rates upon a number of uncertain kinetic and photochemical parameters for iodine species.

1 Introduction

The chemistry of the sunlit troposphere is dominated by the reactions of the hydroxyl radical, OH, which is responsible for initiating the degradation of most hydrocarbons and other species emitted to the atmosphere. Knowledge of atmospheric hydroxyl levels (OH), of related species such as HO_2 (collectively HO_x), and the chemical processes which govern their abundance, is central to explaining current atmospheric trace gas distributions and predicting their likely future evolution.

Interest in the chemistry of the polar boundary layer, and the atmospheric chemistry above the surface of the polar ice sheets and sea ice, has grown in recent years, driven in part by interest in understanding atmospheric evolution through measurements of trace gases in air trapped in ice cores and firn. In addition to climatic information derived from long-lived tracers such as CO_2 levels and various isotope ratios, measurements of sulphur, nitrate and peroxide levels have

all been used to infer historic atmospheric composition (e.g. Wolff, 1995; Legrand and Mayewski, 1997); understanding the chemical environment in which these species are deposited and incorporated in firn/ice, i.e. the background chemistry of the polar boundary layers, is clearly important for such analyses. From the perspective of the modern atmosphere, interest in the polar boundary layer has also been driven by the observation of periodic surface ozone depletion events linked to bromine chemistry in the Arctic, and the recognition that snowpack can act as a source of nitrogen oxides NO and NO$_2$ (collectively NO$_x$), HONO, HCHO and peroxides, amongst other species, thereby modifying the boundary layer composition from what might be expected for regions very remote from pollutant sources (Grannas et al., 2007).

This paper presents a model analysis of boundary layer chemistry based upon observations made in the coastal Antarctic boundary layer during the CHABLIS (Chemistry of the Antarctic Boundary Layer and the Interface with Snow) campaign at Halley Research Station in coastal Antarctica. A zero-dimensional detailed photochemical box model is employed, constrained by observed levels of long-lived chemical species, meteorological and photochemical parameters, to simulate concentrations of short-lived radical species. A particular focus is the model's ability to reproduce the levels and diurnal profiles of HO$_x$ and NO$_x$ measured during the austral summer, and the impact of halogen chemistry upon radical cycling and in situ chemical ozone production/destruction.

2 Context

The first high latitude boundary layer measurements of OH were performed at Palmer Station, a coastal site on Anvers Island, located approximately halfway down the western side of the Antarctic Peninsula (64.0° W, 64.7° S), during the 1993/1994 austral summer using Chemical Ionisation Mass Spectrometry (CIMS; Jefferson et al., 1998). OH concentrations were low, ranging from $(1-9) \times 10^5$ molecules cm^{-3}. Box model simulations, using a model constrained to observed VOC levels (CO, CH$_4$ and C$_2$H$_6$ were the only species found to be important) and radiation agreed well with the OH measurements, if NO levels of 1-5 pmol/mol (ppt) (below the detection limit of the monitor deployed) were assumed. Primary production, O(^{1}D) + H$_2$O, was found to account for over 70 % of the total OH production over the diurnal cycle.

Subsequent studies in the Arctic and Antarctic identified the snowpack as a source of a number of reactive species: HCHO (Sumner and Shepson, 1999; Hutterli et al., 1999), NO$_x$ (Honrath et al., 1999; Jones et al., 2000) and potentially HONO (Zhou et al., 2001) and higher aldehydes (Grannas et al., 2002). Such emissions will significantly alter the anticipated HO$_x$ levels: HCHO and higher aldehydes will act as HO$_x$ sources upon photolysis (and as OH sinks), while

NO$_x$ will drive radical cycling and HO$_2$ to OH conversion, potentially leading to ozone production, and heterogeneous HONO production followed by photolysis will result in a direct source of both NO and OH (Grannas et al., 2007 and references therein).

Measurements of OH performed at South Pole (altitude = 2835 m) found much higher levels of OH than those observed at Palmer Station; average OH concentrations of $(2-2.5) \times 10^6$ cm^{-3} were reported during the austral summers of 1998 and 2000 (Mauldin et al., 1999, 2004). These levels can be compared with the daily maximum levels $(7 \times 10^5$ cm$^{-3})$ from Palmer Station (similar solar zenith angle). The South Pole OH data were consistent with rapid radical cycling driven by snowpack emissions of NO$_x$, the effect of which was enhanced by the low boundary layer height at South Pole station (Chen et al., 2001; Davis et al., 2001). While agreement between observed and modelled OH and HO$_2$ + RO$_2$ levels was satisfactory for moderate levels of NO (ca. 100 pmol/mol in this environment), at lower and higher NO levels the model over predicted the observed OH; moreover inclusion of measured HONO levels in the model led to a large overestimate of the measured NO$_x$, OH and HO$_2$ + RO$_2$ levels (Chen et al., 2004). Subsequent observations of HONO using a photofragmentation-LIF technique found the HONO abundance to be much lower (by a factor of 7) than mist-chamber/ion chromatography data suggested (Liao et al., 2006). Further measurements were performed during the 2003 ANTCI (Antarctic Tropospheric Chemistry Investigation) project, finding comparable OH levels of typically $(1.5-2.5) \times 10^6$ cm^{-3} (Mauldin et al., 2010), with even higher NO levels (up to 1 ppb) than observed previously (Eisele et al., 2008). Box model calculations of OH constrained by observations of longer-lived species systematically overestimated the measured OH levels by a factor of 2–3 with no clear cause for the discrepancy identified (Mauldin et al., 2010).

HO$_x$ have also been measured above snowpack at Summit, Greenland: Sjostedt et al. (2007) used chemical ionisation mass-spectrometry to measure OH radicals and the sum of organic and inorganic peroxy radicals (ΣHO$_2$ + RO$_2$) at the Summit research station (altitude = 3200 m) during summer (June/July) 2003. Median radical levels of 6.4×10^6 cm^{-3} (OH) and 2.2×10^8 cm^{-3} (ΣHO$_2$ + RO$_2$) were observed, much higher than the earlier South Pole observations, which can be explained in part by the lower solar zenith angles and higher humidity and ozone levels at Summit. Model calculations, constrained to observed radical sources including HCHO, H$_2$O$_2$ and HONO were found to replicate the observed peroxy radical levels very well when the HONO source was removed, with a modest overestimate (27%) with the inclusion of HONO. For OH radicals however the measured values were found to be a factor of 2–3 times higher than those modelled, pointing to missing chemical processes (OH sources and/or HO$_2$/RO$_2 \rightarrow$ OH conversion processes). Sjostedt et al. noted that the model:observations

(M/O) ratio was highest during periods of high wind, and when back-trajectory calculations indicated that air masses had recently originated from the surrounding marine boundary layer, and hypothesised that halogen reactions may be responsible for peroxy radical to OH conversion and hence the M/O discrepancy, although no halogen measurements were available during the campaign. Model simulations of these observations (Chen et al., 2007) were able to reproduce the observed peroxy radical ($HO_2 + RO_2$) levels, but again underestimated OH levels by a factor of 2. Primary HO_x sources were found to be $O(^1D) + H_2O$ and photolysis of HCHO and H_2O_2, with snowpack emissions forming a significant source of these, particularly for H_2O_2, while the dominant HO_x sink was the HO_2 self-reaction. As the NO_x levels were lower at Summit than South Pole, overall HO_x abundance was driven by the rates of primary production and termination, rather than NO_x-driven cycling processes.

A wide variation in radical concentrations, and the levels of related species with snowpack sources (NO_x, H_2O_2, HCHO) is thus observed in overtly similar polar environments, probably driven largely by differences in local dynamical factors (stability/boundary layer height) and as a consequence of processes within the snowpack leading to the production of NO_x, HONO and aldehydes amongst others; it is within this context that the radical data from the CHABLIS campaign in coastal Antarctica are analysed here.

Halogen species are also known to be of importance in some polar regions, with bromine chemistry in particular involved in the surface ozone depletion events observed in the coastal areas of both polar regions (Simpson et al., 2007 and references therein). During CHABLIS, the halogen monoxides IO and BrO were observed by DOAS (Differential Optical Absorption Spectroscopy) at levels of up to 20 pmol/mol (Saiz-Lopez et al., 2007a). Halogen chemistry is expected to lead to direct catalytic ozone destruction, and will also perturb the NO_x and HO_x cycles giving rise to indirect effects upon local oxidising capacity; Saiz-Lopez et al. (2008) used an unconstrained 1-dimensional model to calculate a chemical ozone loss rate at Halley of up to 0.55 nmol/mol h^{-1} (ppb h^{-1}), and substantially increased OH and reduced HO_2 levels, by ca. 50% in each case. Subsequently, Bauguitte et al. (2009) have shown that the observed NO_x levels are consistent with a NO_x lifetime of the order of 6 h, shorter than would be anticipated for such a remote location, thought to be a consequence of the hydrolysis of halogen nitrates constituting a significant additional NO_x sink. In this paper, we extend these analyses using all the available observations from the CHABLIS campaign to constrain the model simulations, with a particular focus upon HO_x as the species most sensitive to in situ chemical processing within the Antarctic coastal boundary layer.

3 Measurement overview

The CHABLIS (the Chemistry of the Antarctic Boundary layer and the Interface with Snow) measurement campaign was conducted at the British Antarctic Survey's Halley (V) Research Station, located on the Brunt Ice Shelf off Coats Land, at 75° 35′ S, 26° 39′ W. A full description of the CHABLIS project, site details and measurements performed is given by Jones et al. (2008); pertinent details are summarised here. The base is located on a peninsula of the ice sheet, surrounded by the Weddell Sea to the North around (counter clockwise) to the South West, with the permanent ice front located 15–30 km from the base depending upon direction; the base location is approximately 32 m a.s.l. During the period of the observations used here (January–February 2005), the sea ice cover had almost entirely dissipated. The prevailing wind was from ca. 80 degrees, corresponding to a uniform fetch of several hundred km over the ice shelf. The measurement site, comprising a shipping container housing the LIF instrument for HO_x measurements, and an adjacent Clean Air Sector Laboratory (CASLab) housing the remaining instruments, was located ca. 1 km upwind of the other base buildings (and generators), at the apex of a clean air sector encompassing the prevailing wind direction, within and above which vehicle and air traffic movements were prohibited. Measurements were performed over a 13-month period from January 2004, with an intensive summer measurement campaign, January–February 2005, which included the HO_x measurements considered here.

The observations used in this analysis are summarised in Table 1. OH and HO_2 radicals were measured by laser-induced fluorescence (LIF) spectroscopy, using the Fluorescence Assay by Gas Expansion methodology; full details of the measurements are given in Bloss et al. (2007). The LIF instrument had a sampling height of 4.5–5 m above the snow surface, and was co-located with inlets for measurement of humidity and ozone levels. NO was detected by chemiluminescence and NO_2 was measured following its conversion to NO (photolytic converter) – Cotter et al. (2003)/Bauguitte et al. (2009). The NO_x instrument was housed within the CASLab, and sampled from the laboratory's main manifold, with an inlet height approximately 8 m above the snow surface. Nitrous acid (soluble nitrite) was measured by scrubbing gas-phase HONO into aqueous solution in a mist chamber, followed by derivatisation to 2.4-DNPH and HPLC/ absorbance detection (Clemitshaw, 2006). The halogen monoxide radicals IO and BrO were measured by Differential Optical Absorption Spectroscopy (DOAS); the DOAS instrument and telescope were housed within the CASLab, while a retro reflector array was positioned 4 km due East of the measurement site, with the beam path approximately 5 m above the snow surface. The two species could not be measured simultaneously as they absorb in different spectral regions, and the DOAS spectrometer covered a wavelength range of ca. 25 nm at any given time. Further details of the instrument and

Table 1. Observed chemical climatology of the Coastal Antarctic Boundary Layer during the CHABLIS summer measurement period (January–February 2005).

Species	Technique	Observation Frequency	Mean level	Observed range
OH,	LIF	30 s	3.9×10^5 cm^{-3}	<LOD–2.8×10^6 cm^{-3}
HO$_2$			0.76 pmol/mol	<LOD–3.7 pmol/mol
NO	Chemiluminescence,	1 min	7.3 pmol/mol[1]	<LOD–42.6 pmol/mol
NO$_2$	photolytic NO$_2$ conversion		4.3 pmol/mol[1]	<LOD–34.4 pmol/mol
HONO	Mist chamber/HPLC	15 min	7 pmol/mol	<LOD–38 pmol/mol
IO	LP-DOAS	20–80 min	3.3 pmol/mol	<LOD–7.6 pmol/mol
BrO			2.5 pmol/mol	<LOD–9.0 pmol/mol
NMHCs	GC-FID	Hourly	Note 2	–
O$_3$	UV Absorption	1 min	7.0 nmol/mol	2.6–10.5 nmol/mol
CO	VUV Fluorescence	1 min	34.4 nmol/mol	14.5–57.4 nmol/mol
HCHO	Fluorescence/Hantsch	1 min	127 pmol/mol	<LOD–385 nmol/mol
CH$_4$	Flask Analyses	Monthly	1720 nmol/mol	–
H$_2$			546 nmol/mol	–
H$_2$O	Dew point hygrometer	10 min	9.4×10^{16} cm^{-3}	$(3.1–16.6) \times 10^{16}$ cm^{-3}
Actinic Flux	Spectroradiometer	1–2 min	j(NO$_2$): 9.4×10^{-3} s^{-1} [3]	0.44–23.6×10^{-3} s^{-1}
	2π, periodically inverted		j(O^{1}D): 1.5×10^{-5} s^{-1} [3]	0.0046–5.9×10^{-5} s^{-1}
Temperature	Met. Station	1 min	268.1 K	254.3–275.0 K
Wind Speed	Met. Station	1 min	5.2 ms^{-1}	0–18.8 ms^{-1}

Notes: (1) NO$_x$ values exclude data affected by base generator exhaust, pollution events, (2) See Read et al. (2007) for details of NMHC data, (3) Values stated include upwelling component.

IO/BrO observations are given in Saiz-Lopez et al. (2007a). VOCs (volatile organic compounds) were measured by gas chromatography with flame ionisation detection (GC-FID): ethane – benzene, DMS (Read et al., 2007, 2008). Formaldehyde was measured via scrubbing into sulphuric acid followed by the Hantsch reaction/fluorescence (Aerolaser 4021 monitor; Salmon et al., 2008). VOCs and HCHO were sampled from the CASLab inlet, 8 m above the snow surface. No measurements of oxygenated VOCs (other than HCHO) were attempted – the potential abundance of these species and their influence is considered later. Levels of CH$_4$ and H$_2$ at Halley in January/February 2005 were 1720 and 546 nmol/mol respectively (NOAA Global Monitoring Division flask analyses). Ozone was measured by UV absorption (Thermo 49C) and carbon monoxide by VUV fluorescence (Aerolaser AL5001, calibrated from a ±5% accuracy standard cylinder).

Other environmental parameters used in this study include humidity, determined using a dew-point hygrometer (General Eastern 1311) and solar radiation: actinic flux was measured using a 2–π spectral radiometer (Meteorologie Consult GmbH), periodically inverted to determine the upwelling flux. Meteorological parameters were determined using Campbell Scientific weather stations at various locations around the measurement site – the temperature used in the model analysis corresponds to the LIF instrument inlet height. Boundary layer structure and stability was to

have been determined using a SODAR array which was unfortunately inoperable during the CHABLIS summer measurement period; previous data (König-Langlo et al., 1998; Jones et al., 2008) suggested a typical boundary layer height of 100 m, which is adopted as the initial estimate in this work; the sensitivity of the model results to this parameter are evaluated.

3.1 Data processing/base generator pollution events

All observations were analysed on a 10-min timebase. In the case of high-resolution measurements (HO$_x$, NO$_x$, HCHO, photolysis frequencies, and meteorological parameters) the mean of all observations within each 10-min window was used (where data were available). In the case of low frequency measurements (VOCs; 60–90 min) the data were interpolated. A pollution filter was then applied to all data: Halley obtains its power from a set of generators which were located ca. 1 km from the measurement site. On occasion (10.0% of all observation points) the generator exhaust was sampled at the CASLab site (identified from local wind direction and NO$_x$ levels) and the data were flagged as potentially polluted. Such observations were excluded from all model-observation comparisons reported below. In addition to the base sector pollution events, times at which there were gaps in the dataseries for long-lived species (NO$_x$, O$_3$, CO, HCHO, NMHCs, radiation measurements)

due to instrumental difficulties were excluded from the measurement-model comparison; in total 1963 10-min data points remained, representing ca. 55 % of all HO$_x$ observations.

4 Model description

The HO$_x$-NO$_x$-XO$_x$ interactions were investigated using a zero-dimensional box model, comprising standard inorganic and organic reaction kinetics and photochemistry taken from the Master Chemical Mechanism (MCM) version 3.1 (http://mcm.leeds.ac.uk/). The DMS oxidation scheme used by Sommariva et al. (2006)/Carslaw et al. (1999) was added. A halogen (iodine and bromine) reaction scheme was implemented as described below. The model incorporated a simple representation of heterogeneous processes from the perspective of loss of gas phase species, and dry deposition. The model ran within the FACSIMILE integration package, outputting species for comparison with observations on a 10-minute timestep, with a five-day spin-up period employed for each day simulated.

4.1 Photolysis frequencies

Photolysis frequencies used in the model were taken from the direct observations in the cases of $j(O^1D)$ and $j(NO_2)$ (Jones et al., 2008). Photolysis frequencies for other species were calculated following the algorithms of Hough et al. (1988) as implemented in the MCM (version 3.1), and were then scaled by the ratio of the calculated and observed $j(NO_2)$ values (Sommariva et al., 2006). For species not included in the MCM (those listed in Supplementary Table S1 – iodine and bromine compounds) photolysis frequencies were calculated from the measured values of $j(NO_2)$, using a scaling factor determined as the mean ratio of the photolysis frequency in question to $j(NO_2)$, calculated using clear-sky actinic flux data from TUV (Madronich and Flocke, 1998) averaged over the SZA range appropriate to the CHABLIS summer measurement period, employing the cross sections/quantum yields listed in Table S1. The uncertainty introduced by this approach – using a single scaling factor for all solar zenith angles – was less than 9% for all species listed in Table S1 (with the exception of HI, for which the error was 33%, a consequence of the pronounced short-wavelength contribution to photolysis, but for which photolysis is a negligible sink on the timescale of these simulations). The error introduced by this approach is minimised in this specific case as we are considering (local) summertime only at a high-latitude site above the Antarctic Circle, where the absolute variation in solar zenith angle is relatively small.

4.2 Halogen reaction scheme

The model includes a detailed chemical scheme for halogen (bromine and iodine) inorganic/organic reactions. Gas-phase

kinetic parameters were taken from the literature, drawing upon the NASA/JPL and IUPAC evaluations (Sander et al., 2006; Atkinson et al., 2007) where possible. A number of the kinetic and photochemical parameters are either poorly understood or simply unmeasured, particularly in the case of iodine chemistry; we have estimated these where necessary, as detailed in the notes to Supplementary Table S2, and considered potential variations in the rate and products of some of the key processes in a sensitivity study, including the photolysis quantum yield for OIO (base case 5% I + O$_2$; alternate 100% I+O$_2$); absorption cross sections for IONO$_2$, I$_2$O$_2$, I$_2$O$_3$, I$_2$O$_4$; kinetics/ products of IO + CH$_3$O$_2$ reaction; thermal stability of I$_2$O$_2$, I$_2$O$_4$.

4.3 Heterogeneous processes

Aerosol size distributions were not measured during CHABLIS, so the true surface area, and diffusion/transition regime effects, cannot be calculated. Rather, heterogeneous uptake of reactive gas-phase species is simulated using the free molecular approach, assuming an aerosol surface area of 10^{-7}cm^2 cm^{-3}, based upon typical remote marine levels (von Glasow et al., 2002; Saiz-Lopez et al., 2008); reaction probabilities used are summarised in Supplementary Table S3. Uptake and subsequent hydrolysis of species such as IONO$_2$ and HOI upon aqueous aerosol ultimately leads to re-release of molecular (inter)halogen molecules such as IBr and ICl (Vogt et al., 1999); the implementation of such processes in this model is however difficult considering that (1) we do not know the halogen source strength (precursor compounds) in any case, so have to include a halogen source, which cannot distinguish between snowpack and aerosol production, (2) we do not have aerosol size distribution or composition data to accurately simulate aerosol processes, (3) many of the relevant accommodation coefficients/ reaction probabilities are not known and (4) given the uncertainties in many other parameters (e.g. gas-phase reaction and photolysis frequencies) a more complicated treatment is not justified for the purposes of this study. Uptake to the condensed phase is therefore assumed to lead to permanent removal of the gas-phase species: reactions in the condensed phase are not incorporated. In the model the heterogeneous halogen source will be subsumed within the overall halogen source term; an estimate of its maximum potential magnitude is obtained by assuming that uptake to the aerosol is the rate-limiting step for iodine recycling, which then proceeds with unit efficiency (see comments below). Dry deposition was included for all non-constrained species with a deposition velocity of 0.5 cm s^{-1}.

4.4 Observational constraints

The concentrations of species with a long chemical lifetime relative to HO$_x$ were constrained within the model to the

observed levels – H$_2$, CO, VOCs (CH$_4$, HCHO and NMHCs) and O$_3$; accordingly no entrainment or loss of these species from the boundary layer was considered in the simulation (the required entrainment which would be required to maintain e.g. O$_3$ levels in a free-running simulation is considered below), and the levels inherently incorporate the sum of advected contributions and local snowpack production and depositional loss.

4.5 NO$_x$ and halogen source terms

The model NO$_x$ source term (where used) was proportional to the photolysis frequency of the nitrate anion, j(NO$_3^-$), which was determined as described in Bauguitte et al. (2009). There is evidence for HONO production from sunlit snowpack (e.g. Honrath et al., 1999; Zhou et al., 2001) and measurements of soluble nitrite/HONO were performed during CHABLIS using a coiled scrubber/ derivatisation/ colourimetry method, however the levels observed (mean 7 pmol/mol during the summer measurement period; Clemitshaw, 2006) were not consistent with the HO$_x$ or NO$_x$ observations – as HONO undergoes photolysis on a roughly 10-min timescale to produce OH + NO, and the NO$_x$ lifetime is of the order of 6 hours in this environment (Bauguitte et al., 2009), HONO levels of 7 pmol/mol would lead to in excess of 250 pmol/mol of NO$_x$, over an order of magnitude greater than the levels observed. We do not include a heterogeneous HONO source in the simulation, although HONO production from the snowpack may in reality contribute to a fraction of the NO$_x$ source implemented, and also lead to OH formation – see discussion. A halogen source was also required to replicate the observed IO and BrO concentrations; for the purposes of this work the halogen source was the production of iodine and bromine atoms from the photolysis of a constant concentration of molecular iodine and bromine. The source strengths (NO$_x$ source, and constant levels of I$_2$/ Br$_2$) were manually adjusted to replicate the observed levels – in the case of the NO$_x$ source, to replicate the local solar noon NO level (the NO$_2$ data were not used to constrain the NO$_x$ source), in the case of the IO and BrO data, to replicate the mean maximum XO level observed.

5 Results

5.1 Constrained model simulations of HO$_x$ and halogen oxide levels

Simulations were performed with the full model to assess our ability to reproduce the observed levels of OH, HO$_2$ and the halogen oxides IO and BrO: case A1. The model was constrained to observed NO$_x$, and the halogen source strength was set to replicate the observed IO and BrO concentrations during the summer measurement period (values given in Table 2). The results for IO and BrO are shown in Fig. 1a and

b, respectively: all XO observations within the HO$_x$ measurement period are shown. For IO, the data show a clear diurnal cycle which is found to track the j(NO$_2$) photolysis frequency strongly; the model simulation is able to capture both the magnitude and variation of the IO levels. For BrO, the pattern shown by the data is less coherent, with a number of outliers apparent; nonetheless the model captures the diurnal variation in BrO levels. As the model source is manually adjusted to replicate the observed halogen monoxide levels the general agreement for magnitude is unsurprising, although it is interesting to note that the single, constant halogen source strength factor reproduces the XO observations reasonably well throughout the measurement period.

Figure 2 shows the simulated time series together with all observations for OH and HO$_2$ radicals. The direct influence of solar radiation on the diurnal profile of HO$_x$ is clearly apparent, together with the sub-90° midnight solar zenith angle particularly near the beginning of the data series. The seasonal evolution of OH (with concentrations decreasing toward the end of the measurement period, as the date moves away from the summer solstice) is also apparent. While the model captures the qualitative features of the data series, the absolute levels of HO$_x$ are significantly overestimated. The correlation between modelled and measured values for OH and HO$_2$ are shown in Fig. 3a–c. An unweighted linear regression analysis of all data points returns modelled:observed ratios of 3.7 ± 0.2 and 2.0 ± 0.1 with small positive intercepts of $(3.4 \pm 0.7) \times 10^5$ molecule cm^{-3} and (0.5 ± 0.05) pmol/mol for OH and HO$_2$, respectively. Forcing the analyses through the origin increases the mean modelled:observed ratios to 4.1 ± 0.1 and 2.5 ± 0.05 for OH and HO$_2$, respectively. For both species it appears from Fig. 2 that the level of agreement may improve towards the end of the time series – corresponding (on average) to lower temperatures, lower absolute humidity and lower radiation levels. Regression of the modelled:observed ratio revealed no significant trend for either OH or HO$_2$ with respect to temperature or humidity, but for radiation levels, measured as j(NO$_2$), a positive trend (albeit with considerable scatter) was found for the modelled:measured OH ratio: OH$_{mod/obs}$ = $(480 \pm 320) \times j$ (NO$_2$)/s^1 – (0.6 ± 3.6). Uncertainties are $\pm 2\sigma$ and reflect precision only. While the HO$_2$ data display no significant overall trend, some structure was apparent in the model-measurement ratio vs. j(NO$_2$) correlation plot, with the model performing better at the lowest radiation values.

In the case of OH, no relationship was apparent between the modelled:observed OH ratio and wind speed, local wind direction, temperature, humidity, ozone or measured VOC levels. No change in the modelled:observed OH ratio was apparent with NO$_x$ level, however it is noticeable from Fig. 3a, which is coloured by measured NO$_x$, that both measured and modelled levels were higher at higher NO$_x$ levels, reflecting NO-driven HO$_2$ to OH conversion. While the OH model and observed data display no obvious structure, the HO$_2$ data,

Table 2. NO_x and halogen source strengths, and corresponding surface fluxes, incorporated in model simulations.

	Model source strength /pmol mol^{-1} or /molec cm^{-3}	Peak surface flux X_2 or NO_x/ molec cm^{-2} s^{-1}	24-h mean flux /molec cm^{-2} s^{-1}
Case A1:			
Iodine Source	0.04	4.0×10^9	2.0×10^9
Bromine Source	0.07	1.2×10^9	6.0×10^8
Case B1:			
NO_x Source	3×10^{10}	2.7×10^7	6.5×10^7
Case B2:			
NO_x Source	1.7×10^{11}	1.5×10^8	3.7×10^8
Iodine Source	0.04	4.0×10^9	2.0×10^9
Bromine Source	0.07	1.2×10^9	6.0×10^8

Notes: NO_x production is implemented as [NO_x Source] $\times j(NO_3^-)$. The halogen sources are implemented as $d[X_2]/dt = j(X_2)$ [X_2 source], with a constant value for X_2 source, the "molecular halogen level" (given as a mixing ratio above). Surface fluxes are for I_2, Br_2 or NO_x, and are calculated assuming a 100 m mixed layer depth, and that the contribution from aerosol recycling is zero. See text for scenario definitions.

Fig. 3b and c, appear to fall into two distinct populations, with one cluster close to the 1:1 line and a second, larger group following a higher trend with some apparent curvature. No trends in the HO_2 model:observed ratios were observed with wind speed, temperature, humidity, ozone or VOC levels, however the data in the former (lower) group correspond to low NO_x levels and high solar insolation (the data in Fig. 3b are coloured by NO_x level), and only occurred when the local wind direction was from the east-south sector (i.e. the Clean Air Sector, corresponding to continental, ice sheet direction), Fig. 3c. Whenever the local wind direction was from the west (i.e. having recently crossed the Weddell Sea, open at this time), the modelled:measured ratio lay in the higher group. The relationships are not exclusive – that is, low NO_x and/or continental air seems to be a necessary but not a sufficient condition for the modelled:observed ratio to lie within the lower (better agreement) group. Most observations with northerly local wind direction are excluded owing to base sector air pollution effects as described previously. The halogen monoxide observations are too limited to permit the equivalent correlations to be explored, but we note that both the observed XO levels, and the halogen source term in the model, scaled with radiation – $j(NO_2)$ – so the trends noted above may be a response to IO and BrO chemistry, rather than directly to sunlight *per se*. This possibility, together with other factors potentially affecting the model:measurement ratio, is explored below.

The mean observed HO_2:OH ratio of 46 was in good agreement with the mean modelled value of 44 (values are means of central 80% of all values). The correlation between the observed and modelled HO_2:OH ratio displayed no significant dependence upon temperature, wind speed, wind direction, humidity, ozone or VOC levels, but did vary with NO_x, as shown in Fig. 3d. There is a slight ten-
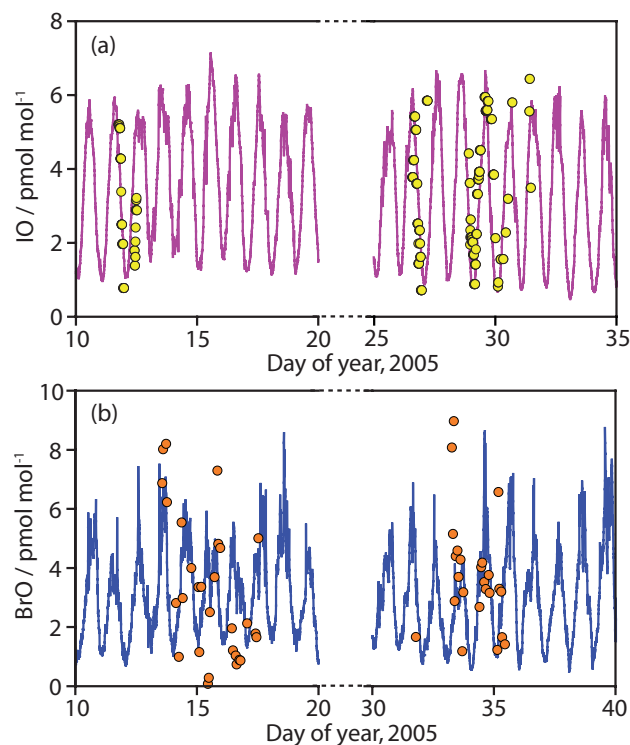
Fig. 1. (a) Observed and modelled IO and (b) Observed and modeled BrO mixing ratios as a function of day of year, 2005.

dency for the modelled HO_2:OH ratio to exceed that observed with increasing NO_x, and a number of significant model overestimates of the ratio at the lowest NO_x mixing ratios. The data in Fig. 3d are coloured by radiation level, measured as $j(NO_2)$ – the model overestimates of the observed HO_2:OH ratio occur almost exclusively at the lowest

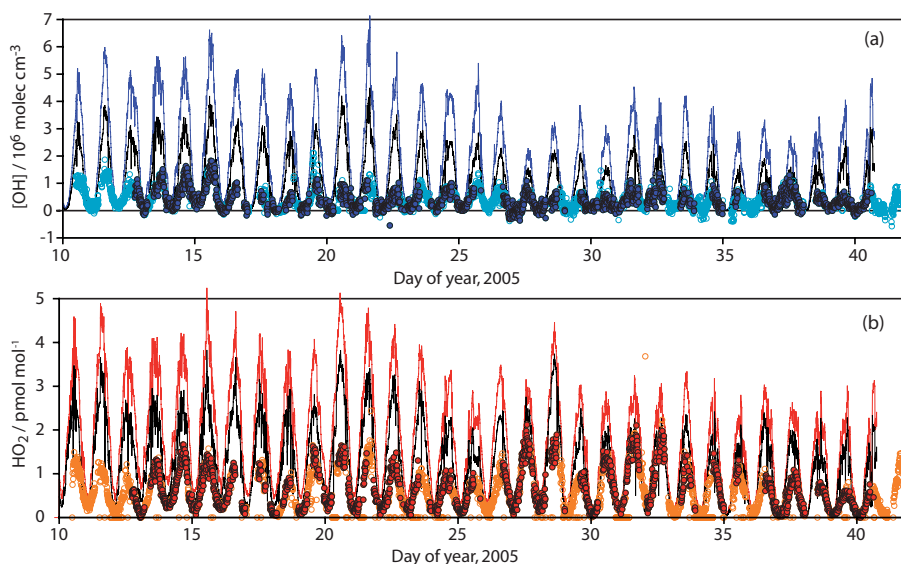**Fig. 2.** Observed and simulated times series of **(a)** OH concentrations and **(b)** HO$_2$ mixing ratios. Open circles: all HO$_2$ observations. Filled circles: observations for which all other data present, as used in model-measurement comparisons. Blue line/red lines: model case A; black lines: model case C.

values of j(NO$_2$). This would correspond to more rapid atmospheric HO$_2$-to-OH conversion than is predicted at times when NO$_x$ levels are low, and when solar radiation is low (i.e. when NO$_x$ tends towards NO$_2$). The modelled and observed (local) noon HO$_x$ levels are compared in Table 3, which is further subdivided into all data (with available supporting observations), and the subset of those data for which IO was directly observed (i.e. as shown on Fig. 1). The values reflect the behaviour apparent in Fig. 2; while the modelled:observed ratio shows some improvement for the subset of observations for which IO measurements were available, this reflects the fact that the distribution of these was biased towards the end of the campaign, where the overall agreement was better.

5.2 Radical budgets: factors controlling NO$_x$ and HO$_x$ levels

In order to investigate the dependence of the results upon the chemical (kinetic and photochemical), physical (aerosol surface area, boundary layer height) and model assumptions, and to try to identify those factors which might have the greatest bearing upon the model overestimate of HO$_x$ levels, a number of sensitivity studies were performed. To simplify the scenario considered, a *simplified model* (B) was used in which the VOC scheme was limited to C$_1$ species (methane and its degradation products), rather than the *full model* (A, as used to generate Figs. 1–3). The principal motivation behind use of the simple model was to simplify the budget analysis and sensitivity studies, while a further consideration was that kinetic data are simply unavailable for most of the radical – radical reactions involving halogen species and organics

over C$_1$ in size. For model B, the VOC scheme was reduced to CH$_4$-only degradation reactions (plus inorganic/halogen chemistry), and the CH$_4$ input level was increased (by a diurnally varying amount) such that the total OH reactivity was maintained, i.e. extra CH$_4$ was added to replicate the magnitude of the total NMHC OH sink – this represented an increase of approximately 550 nmol/mol on top of the true level of 1720 nmol/mol. Under this scenario, the maximum OH and HO$_2$ levels calculated from the simple model (B) were within 6 and 2% respectively of those calculated using the (mean) full set of NMHC species observed with model A – reflecting the minimal contribution of NMHCs to the total OH reactivity sum (CH$_4$, CO and H$_2$ comprised over 96% of the total measured OH sink). The model was constrained to the mean diurnal profiles of long-lived species (HCHO, CO, O$_3$, H$_2$O vapour), temperature and photolysis frequencies obtained from the summer measurement period.

5.2.1 Diurnal NO$_x$ profile and halogen influence on NO$_x$ lifetime

Figure 4 shows the mean diurnal observed NO$_x$ levels, and the results from two model simulations. The observed NO and NO$_2$ levels follow a sinusoidal profile, varying from 1.9 pmol/mol at night to a maximum value of around 14.1 pmol/mol during the day for NO, and from 3.0 pmol/mol in the early morning to 12.8 pmol/mol in the evening for NO$_2$. The first model simulation (case B1) included a NO$_x$ source manually tuned to replicate the mean NO level observed at local noon), but no halogen source. The resulting simulations failed to capture the NO$_x$ diurnal profile; the calculated NO$_x$ lifetime was much longer than that observed.

Table 3. Comparison of modelled and observed mean daily maximum OH and HO$_2$ values

	OH/10^6 cm^{-3}	OH M/O	HO$_2$/nmolmol^{-1}	HO$_2$M/O
Whole Timeseries				
Observed	0.98 ± 0.30		1.10 ± 0.33	
Model A	3.7 ± 1.21	3.8	3.12 ± 0.79	2.8
Model C	2.24 ± 0.77	2.3	2.26 ± 0.58	2.1
IO Observations Only				
Observed	0.84 ± 0.22		1.30 ± 0.38	
Model A	2.77 ± 0.51	3.3	2.87 ± 0.49	2.0
Model C	1.70 ± 0.25	2.0	2.31 ± 0.56	1.8

Uncertainties are $\pm 1 \sigma$.

Inclusion of a halogen source with a magnitude manually tuned to replicate the mean IO and BrO levels, and associated readjustment of the NO$_x$ source (case B2), resulted in a much better replication of the diurnal NO$_x$ profile (Fig. 4), as a consequence of the much shorted NO$_x$ lifetime (ca. 6 h, dominated by the heterogeneous hydrolysis of iodine and bromine nitrate – Bauguitte et al., 2009). The NO$_x$ and halogen source strengths as implemented in the model under the various simulations, and equivalent surface fluxes, are summarised in Table 2.

The principal sources and sinks of NO$_x$ (defined as NO + NO$_2$) in the model are shown in Fig. 5a (corresponding to case B2, with halogens). The halogen reactions dominate the NO$_x$ fluxes – in particular, the removal of NO$_x$ through formation of iodine and bromine nitrite and nitrate. The photolysis of IONO$_2$ and BrONO$_2$ forms NO$_3$ (Supplementary Table S1; Atkinson et al., 2007; Joseph and Plane, 2007), accounting for the major NO$_x$ production term from NO$_3$ photolysis apparent in Fig. 5a. The impact of the halogen species as a permanent NO$_x$ sink, rather than reservoir, is determined by the removal rate of (in particular) the halogen nitrate species through heterogeneous reaction and deposition. This is shown in Fig. 5b, showing the major sources and sinks for NO$_y$, defined here as NO$_y$ = NO + NO$_2$ + NO$_3$ + 2N$_2$O$_5$ + PNA + HONO + RNO$_3$ + RO$_2$NO$_2$ + XNO + XNO$_2$ + XONO$_2$(HNO$_3$ is excluded as its (gas-phase) chemical lifetime is long compared with the duration of the simulations). The role of HONO may be underestimated here as the model only includes that formed through termolecular OH + NO recombination, with no snowpack HONO source (see above) – however introduction of such a source would offset the model NO$_x$ source shown as the dotted line in Fig. 5a and b, and cause further overestimate of HO$_x$ levels. The heterogeneous (and deposition) sinks may be overestimated as loss to aerosol is assumed to be irreversible here while in reality recycling mechanisms exist; however given that both the aerosol surface area and boundary layer height are estimated a more sophisticated treatment is not warranted here. Finally, the importance of CH$_3$ONO$_2$

may be overestimated in Fig. 5a, as CH$_4$ levels have been artificially elevated by ca. 20% above their true level in this scenario, although higher alkyl nitrate yields would be expected for larger NMHCs in the real atmosphere.

The integrated loss of NO$_y$ from heterogeneous loss and dry deposition of the halogen nitrates is 1.4 times that from formation of HNO$_3$; that is, the presence of the halogen species reduces the lifetime of active nitrogen species by more than a factor of 2. This result highlights the importance of the rates of photolysis and thermal decomposition for the XNO, XNO$_2$, XONO$_2$ species for quantitative prediction of NO and NO$_2$ levels in high halogen – low NO$_x$ environments such as Halley. Figure 5 also shows how the sink for NO$_x$ is dominated by the conventional formation of HNO$_3$ during the middle of the day (at least, when solar zenith angles are lowest and photolysis frequencies highest), but at "night" the halogen species dominate the NO$_x$ sink – reflecting the greater reduction in OH at high solar zenith angles compared with IO and BrO which are (in this simulation at least) produced from long-wavelength photolysis of molecular halogen compounds – other potential halogen source compounds in the Antarctic boundary layer, such as alkyl iodides, are also likely to exhibit the same dependence upon visible/ long wavelength actinic flux. The in situ chemical ozone loss rate calculated under scenario B2 ranged from 0.03 to 1.14 nmol/mol h^{-1}, with a 24-h mean value of 0.51 nmol/mol h^{-1}. Ozone loss was dominated by iodine reactions (72%) followed by bromine (28%). The in situ chemical ozone loss calculated is smaller than the depositional loss rate (e.g. a mean loss rate of 1.2 nmol/mol h^{-1} is calculated for a 100 m boundary layer height and a 0.5 cm s^{-1} deposition velocity).

5.2.2 Diurnal HO$_x$ profile and halogen influence on HO$_x$ levels

The simulated mean diurnal HO$_x$ profiles under scenario B2 significantly overestimated the observed mean levels, by factors of 1.1–7.7 (mean 4.8) and 2.2–3.7 (mean 2.9) for OH
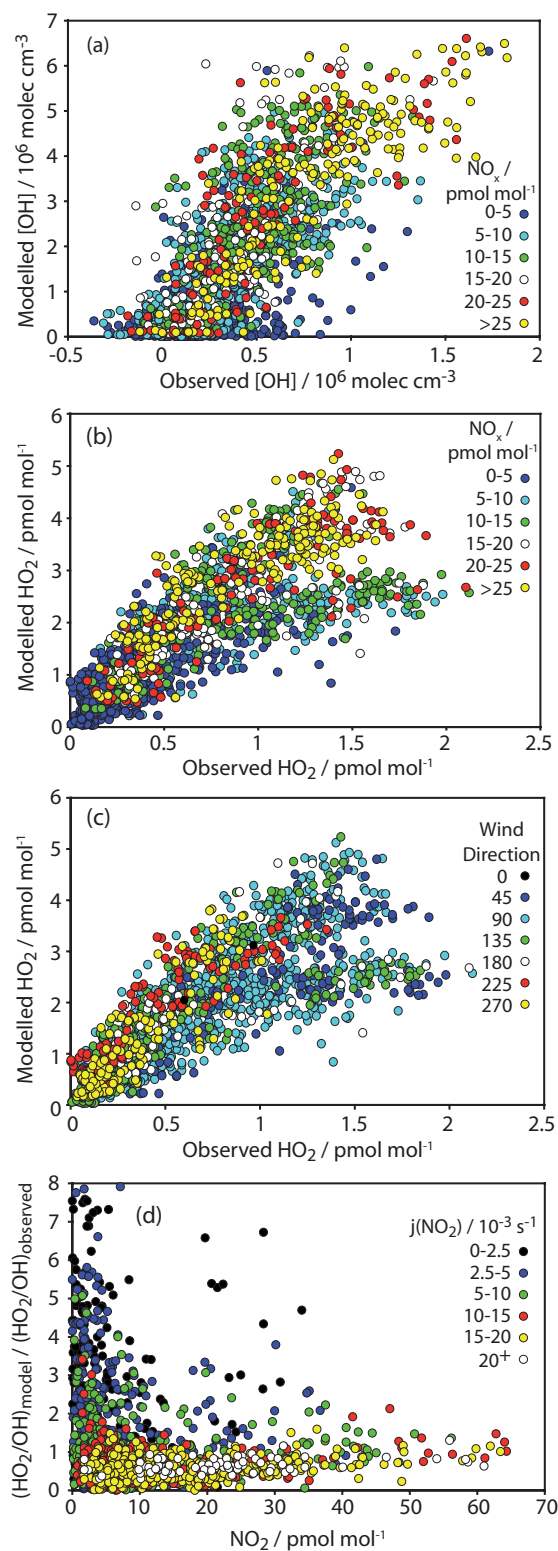
Fig. 3. (a) Modelled vs. observed OH, coloured as f(NO$_x$); **(b)** Modelled vs. observed HO$_2$, coloured as f(NO$_x$); **(c)** Modelled vs. observed HO$_2$ coloured by wind direction (legend denotes centre of 45° sector, expressed in degrees from North) and **(d)** Ratio of modelled to observed HO$_2$:OH ratio as a function of NO$_2$, coloured according to j(NO$_2$).
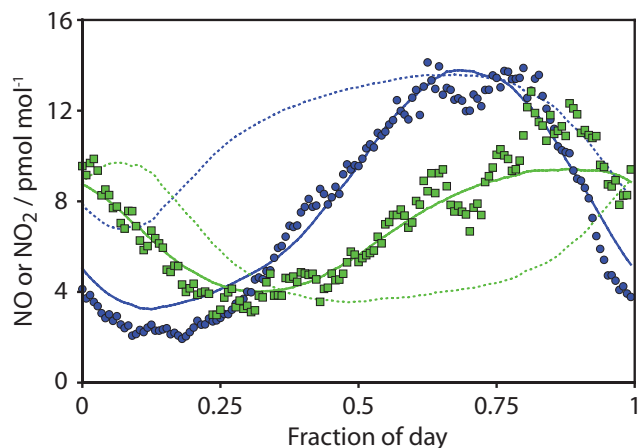

Fig. 4. Mean diurnal measured NO (blue circles) and NO$_2$ (green squares) together with modelled equivalents under case B1 (broken lines; no halogen chemistry) and case B2 (solid lines; halogen source added). In each case the model NO$_x$ source strength was empirically optimised to replicate the peak NO level.

and HO$_2$, respectively, as shown in Fig. 6a. In both cases, the model performed best when photolysis frequencies were lowest. The individual production/ loss terms were evaluated for each of OH and HO$_2$, and for the wider HO$_x$ family. Supplementary Figs. 1a and b show the modelled OH and HO$_2$ production/removal fluxes for the B2 scenario. For OH, production is dominated by photolysis of the hypohalous acids HOI and HOBr, followed by reaction of HO$_2$ with NO, and primary production, O(^{1}D) + H$_2$O. As the source of HOI and HOBr is IO/BrO + HO$_2$, OH production processes are dominated (90.0% of the total) by radical cycling from HO$_2$. OH sinks are reaction with CH$_4$, CO, H$_2$ and HCHO, followed by reaction of OH with OIO (which undergoes photolysis with a 5% quantum yield in the base-case simulation/ halogen mechanism – see discussion below). In the case of HO$_2$, production is dominated by reaction of OH with CO, followed by CH$_3$O + O$_2$ (i.e. OH-initiated oxidation of CH$_4$ followed by CH$_3$O$_2$ + NO, plus a contribution from CH$_3$OOH photolysis). HCHO is major source of HO$_2$, with bromine-initiated formaldehyde oxidation a significant contributor (of the HCHO-related HO$_2$ sources, Br + HCHO accounts for 35% of the total; when considered as an overall HO$_x$ source, Br + HCHO accounts for 46% of the total HCHO-related radical production). Photolysis of peroxides provides a further significant contribution to HO$_x$ production. The major sink for HO$_2$ is overwhelmingly reaction with IO (63% of the total), followed by reaction with BrO and NO, and the termination peroxy self- and cross-reactions.

A clearer picture of the balance between initiation, propagation and termination steps is obtained from consideration of the major sources and sinks for all short-lived HO$_x$ species and their temporary reservoirs. As the halogen
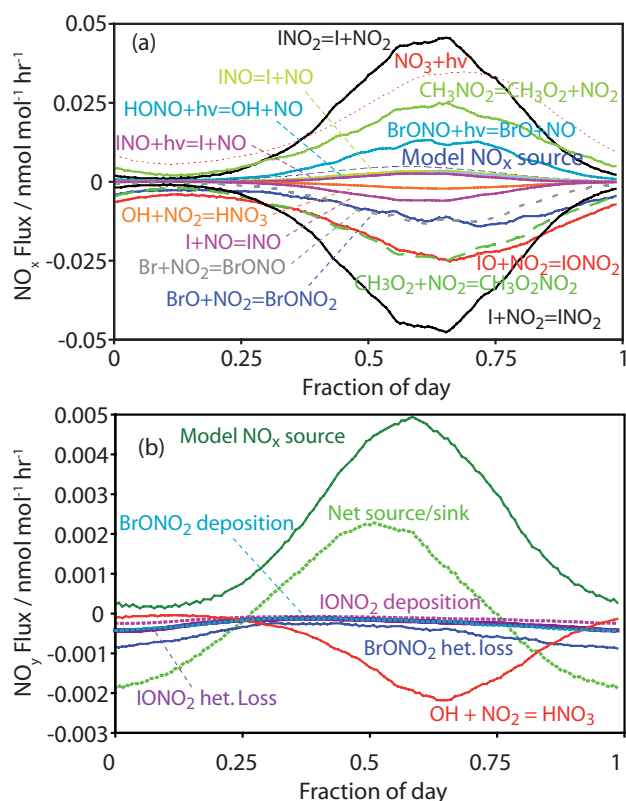
Fig. 5. Diurnal variation in modelled production and loss for **(a)** NO$_x$ and **(b)** NO$_y$. Panel (a), major source and sink processes for NO$_x$ (here defined strictly as NO$_x$ = NO + NO$_2$ only) for model case B2. The NO$_3$ contribution (red dashed line) arises here from photolysis of IONO$_2$ and BrONO$_2$, offsetting their sink role, rather than NO$_2$ + O$_3$ reactions. Panel (b), major source and sink contributions to NO$_y$ calculated for model scenario B2, plus net NO$_y$ production/removal (dashed line). NO$_y$ defined as NO$_y$ = NO + NO$_2$ + NO$_3$ + 2N$_2$O$_5$ + HONO + PNA + CH$_3$NO$_3$ + CH$_3$O$_2$NO$_2$ + XNO + XNO$_2$ + XNO$_3$.

Fig. 6. (a) Observed and modelled mean diurnal OH and HO$_2$ levels. Mean diurnal observed and modelled OH concentrations (blue squares, left axis) and HO$_2$ mixing ratios (red circles, right axis) together with model simulations for scenarios B2 (solid lines) and C (dotted lines); see text for details. **(b)** Modelled ΣHO$_x$ + BrO$_x$ production and removal fluxes. Dotted lines indicate processes involving halogen species.

and HO$_x$ chemistry are closely coupled, the pertinent chemical family to consider is HO$_x$ + BrO$_x$ radicals (iodine species do not react with stable hydrocarbons and so do not provide an additional source of HO$_x$ radicals; rather they affect the speciation of compounds within the HO$_x$ and BrO$_x$ families, in addition to influencing levels of NO$_x$, O$_3$ etc.). For a HO$_x$ + BrO$_x$ family, which we define as (OH + HO$_2$ + CH$_3$O$_2$ + HONO + PNA + HOI + 2HOBr + Br$_x$O$_y$), the production/ removal budget is shown in Fig. 6b. Production is dominated roughly equally by O(^{1}D) + H$_2$O, HCHO photolysis and Br$_2$ photolysis (Br + HCHO); removal by the conventional (low-NO$_x$) termination routes of peroxy radical self- and cross-reactions together with a number of halogen-mediated processes which cumulatively represent ca. 40% of the total ΣHO$_x$ sink: loss of HOBr through deposition and reaction with OH accounts for 11 and 5% of the total loss respectively. Iodine species also provide
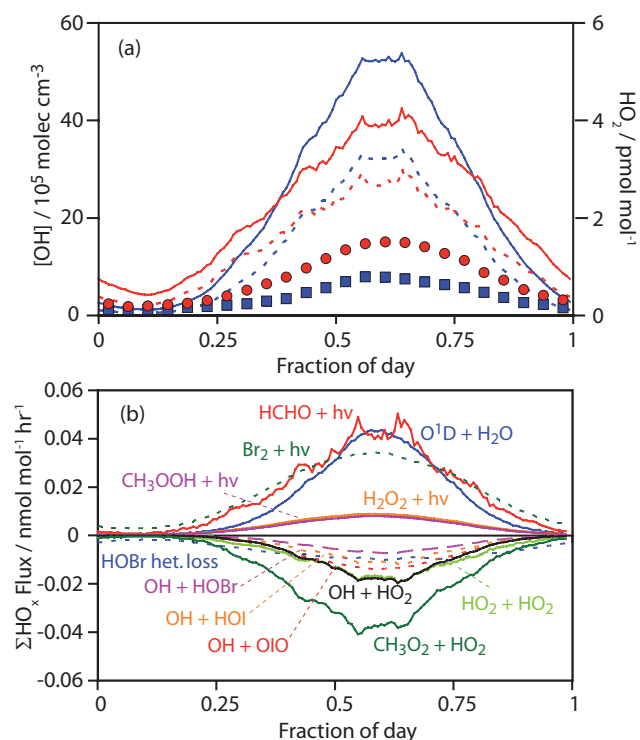
significant HO$_x$ sinks through reactions of OH with HOI and with OIO (7 and 9% of the total sink, respectively). If the CH$_3$O$_2$ + IO reaction were to produce non-radical products, this process would represent an additional HO$_x$ sink of comparable magnitude to the HO$_2$ self-reaction, while the OIO levels simulated (and hence flux through the OIO + OH reaction) are strongly dependent upon details of the I$_x$O$_y$ (photo)chemistry – both possibilities are discussed below.

5.3 Sensitivity to model kinetics and photochemistry

A number of aspects of the halogen chemical kinetic and photolytic scheme are rather uncertain, as a consequence of a paucity of/disagreement between the available laboratory studies. A sensitivity study was performed to examine the dependence of the model outputs upon selected aspects of the halogen, particularly iodine, chemistry, and other model parameters/conditions (e.g. boundary layer height, aerosol surface area). Individual aspects of the chemical scheme were altered in isolation, thus the results do not determine the overall uncertainty but rather indicate which of the processes considered to be least well defined actually have significant

leverage upon the simulated radical levels. The parameters investigated were selected on the basis of either their known measurement uncertainty (or absence), such as the aerosol surface area, or the existence of major uncertainties in laboratory measurements of the kinetics and photochemistry.

The simplified model (B) was used, constrained to observed diurnal mean levels of CO, O$_3$, HCHO, H$_2$O, and physical/ meteorological parameters, together with the observed NO and NO$_2$. This allows the use of simple metric (observed vs. measured HO$_x$) to assess the impacts of changes to the chemical scheme, disaggregating this from effects of changes in the NO and NO$_2$ levels. For each run, the halogen source strengths were re-adjusted to replicate the observed mean diurnal IO and BrO profiles, and the change in levels of OH, HO$_2$ and in situ ozone loss rate at local solar noon were determined. In a second set of experiments, the halogen sources were not adjusted from their nominal values (Table 2, case 2), and the effects upon predicted ozone loss rate for each change was determined. The first approach corresponds to a measure of the uncertainty in modelled HO$_x$ levels (and ozone production/loss) which would result from a situation in which inorganic halogen species concentrations are known (e.g. IO and BrO levels), while the second case assesses the confidence in predicted ozone loss rates for a scenario in which just the halogen source strength is known (e.g. from measurements of halogen precursor abundance), i.e. the uncertainty resulting from limitations in our understanding of the in situ processing rather than of the simulation boundary conditions.

The changes tested were model physical conditions (boundary layer height (BLH), nominally 100 m, and aerosol surface area (ASA), nominally 1×10^{-7} cm^2 cm^{-3}, variations in the rate constant and products for the IO + CH$_3$O$_2$ reaction (nominally 2×10^{-12} molec^{-1}cm^{3}s^{-1} and formation of CH$_3$O + IOO, assumed to lead directly to HCHO + HO$_2$ + I in the boundary layer environment – see Supplementary Table 2, Note 7), the quantum yield for I atom production from OIO photo-absorption (base case Φ_{I+O_2} = 0.05, Φ_{OIO} = 0.95), photolysis frequencies for IONO$_2$, I$_2$O$_2$, I$_2$O$_3$ and I$_2$O$_4$ (all assumed to be equal to j(IONO$_2$), as determined using Joseph et al. (2007) absorption cross sections in the base case) and thermal decomposition rates for I$_2$O$_2$ and I$_2$O$_4$, for which the base case rate constants were 10 s^{-1} and 0.1 s^{-1}.

The changes and results obtained are summarised in Table 4, and plotted on Fig. 7. It is apparent that significant changes in HO$_x$ levels result from increasing the model aerosol surface area (adjustment 2), through increased heterogeneous loss of HOI, HOBr and HO$_2$ (Fig. 6d). Similar conclusions would follow from increasing the reaction probabilities for heterogeneous loss of these species, which are poorly known (Supplementary Table S3). The calculated ozone destruction rate also decreases, as the rates of the XO + HO$_2$ catalytic cycles are reduced. Boundary layer

height changes had minimal impact upon modelled OH and HO$_2$ levels, unsurprisingly given their short lifetimes and the fact that the simulations were constrained to observed levels of longer lived species, however modelled ozone loss (which incorporated deposition) was increased.

Recent studies of the rate constant and products for the IO + CH$_3$O$_2$ reaction are in disagreement, with the rate varying by a factor of 30. Changing from the base-case scenario for the reaction (slower kinetics, products representing radical cycling and ozone destruction i.e. CH$_3$O$_2$ + IO $\rightarrow$ $\rightarrow$ HCHO + HO$_2$ + I) to the faster rate and formation of stable products (e.g. HCHO + HI + O$_2$), resulted in a 30–40% reduction in calculated OH and HO$_2$ levels, arising from a combination of the direct removal of ΣHO$_x$ and the production of HI, acting as an OH sink. We note that some care is needed to interpret the results with respect to ozone as for example details of the photolytic fate of OIO will change the impact of producing OIO vs. IOO from this reaction. The OIO photolysis quantum yields exerted a moderate influence upon the modelled HO$_x$ levels (a variation of $\pm$10%) but dramatically increased the calculated instantaneous chemical ozone destruction rate, when halogen levels were constrained by source strength rather than by XO level, by up to 145% for the change from Φ_{I+O_2} = 0.05 to 1. Recent laboratory data indicate that the high I atom yield is likely to be correct (Gómez-Martín et al., 2009), implying that rather large changes in calculated ozone loss rate may result from similar model analyses, depending upon the data available regarding the halogen abundance (XO levels or halogen source strength). Increasing photolysis frequencies for IONO$_2$ and the higher iodine oxides made little difference under the conditions of these simulations (constrained to observed NO$_x$), the former parameter in particular would be expected to strongly affect NO$_x$ (and hence HO$_x$) levels in a NO$_x$-source-constrained scenario. Similarly, altering the thermal stability of I$_2$O$_2$ and I$_2$O$_4$ did not significantly affect HO$_x$ levels or calculated ozone loss rate.

6 Discussion

6.1 Modelled – observed HO$_x$ trends and correlations

The base-case model was able to replicate the observed variations in the halogen oxides IO and BrO quantitatively well, and reproduced the qualitative behaviour of OH and HO$_2$, including the diurnal and seasonal trends, but significantly overestimated the observed levels. The observed:modelled OH ratio showed some correlation with radiation levels, with the model performing better at lower values of j(NO$_2$) – also apparent as the model performed better towards the end of the time series. The model performance for OH did not vary with NO$_x$ levels, with the observed trend of higher OH observed at higher NO$_x$ levels simulated. For HO$_2$, the modelled:measured correlation plots display a set of data

Table 4. Model sensitivity study.

Number	Change	Percentage change in...			
		OH	HO$_2$	$-d[O_3]/dt$	$-d[O_3]/dt$ FS
0	Reference Run	0.0	0.0	0.0	0.0
1	ASA$=10^{-8}$ cm^{-1}	2.6	1.0	2.4	5.0
2	ASA$=10^{-6}$ cm^{-1}	-30.8	-27.4	-4.9	-19.4
3	BLH$=50$ m	-0.5	-0.5	52.5	52.5
4	BLH$=150$ m	0.1	0.2	-17.7	-17.7
5	IO+CH$_3$O$_2$→HCHO+HO$_2$+OIO $k=2\times10^{-12}$ molec^{-1} cm^3 s^{-1}	-0.3	0.5	-0.6	-0.6
6	IO+CH$_3$O$_2$→HCHO+HI+O$_2$ $k=2\times10^{-12}$ molec^{-1} cm^3 s^{-1}	-5.6	-5.4	-0.5	-0.5
7	IO+CH$_3$O$_2$→HCHO+HO$_2$+I $k=6\times10^{-11}$ molec^{-1} cm^3 s^{-1}	12.9	21.5	6.1	6.1
8	IO+CH$_3$O$_2$→HCHO+HO$_2$+OIO $k=6\times10^{-11}$ molec^{-1} cm^3 s^{-1}	4.2	19.1	4.5	-2.3
9	IO+CH$_3$O$_2$→HCHO+HI+O$_2$ $k=6\times10^{-11}$ molec^{-1} cm^3 s^{-1}	-35.4	-29.7	-1.7	-1.7
10	Φ(OIO+hv→I+O$_2$)=0.0025	-10.5	-3.7	0.2	-25.1
11	Φ(OIO+hv→I+O$_2$)=0.005	-9.4	-5.5	3.0	-23.3
12	Φ(OIO+hv→I+O$_2$)=0.5	10.2	1.3	3.1	96.0
13	Φ(OIO+hv→I+O$_2$)=1	10.9	2.1	2.4	145.0
14	j(IONO$_2$)$\times10$	0.0	0.0	0.1	0.1
15	j(I$_2$O$_2$)$\times10$	0.0	0.0	0.1	0.1
16	j(I$_2$O$_3$)$\times10$	0.7	-3.3	2.9	2.9
17	j(I$_2$O$_4$)$\times10$	0.1	-3.1	3.4	3.4
18	k(I$_2$O$_2$→IO+IO)=5 s^{-1}	-0.3	0.9	-0.5	-0.5
19	k(I$_2$O$_2$→IO+IO)=20 s^{-1}	0.1	-0.5	0.5	0.5
20	k(I$_2$O$_4$→OIO+OIO)=0.05 s^{-1}	-0.1	2.1	-2.1	-2.1
21	k(I$_2$O$_4$→OIO+OIO)=0.2 s^{-1}	0.0	-3.3	3.6	3.6

Notes: FS = Fixed Sources, i.e. NO$_x$ and halogen sources held constant, not re-optimised to reproduce the CHABLIS observations.

which are close to agreement, and which are only found at lower NO$_x$ mixing ratios, and when the wind is from the easterly, continental direction, and a second, larger group which follow the general trend of significant model overestimate, and which include data for all wind directions but at largely higher NO$_x$ levels (in the context of Halley, high is over 15 pmol/mol). At the measurement site, westerly and northerly air will have been exposed to the Weddell Sea (15–30 km distant), which was open water at the time of the measurements, while easterly and southerly directions correspond to the Brunt ice shelf, and eventually (at a distance of several hundred km) the continental rise. Marine sources are anticipated for DMS and its degradation products (shown to be a minor contributor to OH reactivity, < 1% – Read et al., 2008), and potentially for the halogen species (Simpson et al., 2007). The observed NO$_x$ levels did not display any statistically significant variation with local wind direction (after filtering to remove base air contamination). Our model sce-

nario has no directional dependence to the halogen source, so may underestimate the halogen influence when air originated from a westerly or northerly (marine) direction, and overestimate the true levels during easterly and southerly flows (as was observed for the full-year iodine and bromine monoxide data series by Saiz-Lopez et al., 2007). As the major model sink for HO$_2$ is reaction with IO, followed by BrO and NO, the true halogen levels being higher that those simulated under maritime conditions could account for some of the model overestimate of HO$_x$, and would support the proposed marine source for these species (Saiz-Lopez and Boxe, 2008). The mean modelled HO$_2$:OH ratio is close to that observed (44 vs. 46), suggesting that the (ratios of) model OH – HO$_2$ interconversion fluxes are approximately correct. These are dominated by OH + CO/ OH + CH$_4$, and the HO$_2$ + IO, HO$_2$ + BrO and HO$_2$ + NO reactions (Fig. 6b). The ratio of modelled to observed HO$_2$:OH ratios increase at low NO$_x$ levels (that is, the model performs less well, simulating too
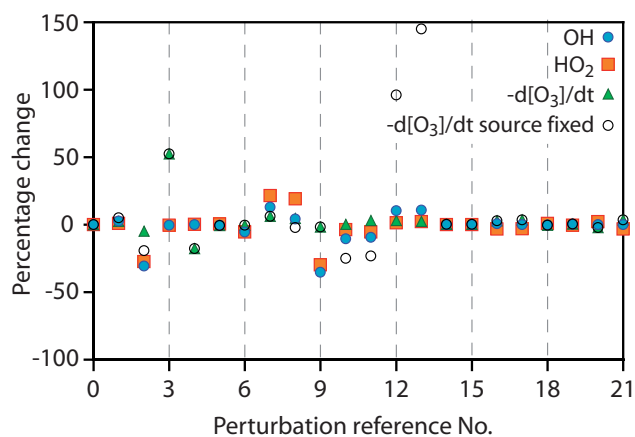
Fig. 7. Percentage change in modelled maximum OH (blue circles) and HO$_2$ (red squares) levels, and ozone loss rate (green triangles) for perturbations 1–21 (Table 4) of the model scheme, and change in ozone loss rate under the assumption of a fixed halogen source strength (open circles); see text for details.

high an HO$_2$:OH ratio; Fig. 3d), possibly suggesting that the halogen-mediated processes play a larger role than is simulated at low NO$_x$ levels, and fitting with the pattern of HO$_2$ modelled: observed ratio NO$_x$ dependence mentioned above – although a direct response to e.g. halogen nitrate stability is unlikely as the model was constrained to reproduce the observed XO levels. The relatively low HO$_2$:OH ratio demonstrates the role of XO radicals driving HO$_2$-to-OH conversion: in other low-NO$_x$ environments, rather higher ratios have been reported, e.g. 76 and 90–137 in the Western Pacific boundary layer (Kanaya et al., 2001) and Pacific free troposphere (Tan et al., 2001), respectively, while lower values have conventionally been associated with polluted environments (e.g. 15 – New York City, Ren et al., 2003; 15–200, Mexico City; Shirley et al., 2006).

6.2 Halogen abundance and sources

The model was able to replicate the general observed diurnal variation in the halogen oxides, IO and BrO, reasonably well (particularly for IO, for which the data is less scattered, and which exerts the larger influence upon OH and HO$_2$) although the dataset is too sparse to test the wind direction dependence postulated above. The model approach neglects halogen recycling via aerosol: under the conditions used, if we were to assume aerosol-mediated halogen recycling proceeded with 100% efficiency at a rate limited by uptake of the gaseous halogen species (i.e. up to I$_2$O$_4$ in this scheme), we would obtain mean iodine and bromine sources of 5.0×10^4 and 8.9×10^4 halogen atoms cm^{-3} s^{-1}, equivalent to 13 and 75% respectively of the implemented model source strengths. Including those iodine species assumed to partition directly to aerosol (PI$_1$–PI$_4$, see Supplementary Table S2), the calculated mean aerosol iodine source strength

would become 3.0×10^5 atoms cm^{-3} s^{-1}, equivalent to 76% of the model source implemented. Considering the uncertainty in the heterogeneous uptake rates, estimated aerosol surface area and the likelihood of some degree of halogen amplification (as is known to occur in the base of bromine; Vogt et al., 1999), aerosol-mediated halogen recycling may in fact be the dominant source of the halogen species observed at Halley, if it proceeds with sufficiently high overall efficiency. Previous studies have determined that the timescale for halogen release is sufficiently rapid (10–15 min in the case of sea-salt aerosol; McFiggans et al., 2000). The calculated lifetime for the gas-phase inorganic iodine species under the chemical scheme adopted here is of the order of 10 min (a mean value of 820 s calculated, although this varies significantly with the overall halogen level through the day as a consequence of non-linearities in the IO/OIO recombination chemistry), dominated by the flux through the I$_2$O$_4$ + O$_3$ reaction). This is substantially shorter than the lifetime with respect to dry deposition (5.5 h calculated here) and much shorter than the distance/ airmass transit time from likely coastal halogen sources, indicating that either large iodine sources exist local to the Halley site, or that a substantial fraction of the iodine which ends up as I$_2$O$_5$ and larger species may in fact be readily recycled to gas-phase inorganic iodine. This in turn may mean that local wind direction might be expected to be a less dominant factor in determining iodine levels at the Halley site – counter to the arguments above. Saiz-Lopez et al. (2008) have applied a 1-dimensional model to the CHABLIS halogen observations, and draw similar conclusions regarding iodine sources and recycling: they were able to reproduce the summertime IO and BrO abundance with iodine and bromine source strengths of 1×10^9 atoms cm^{-2} s^{-1} and 2×10^8 molecules cm^{-2} s^{-1}, factors of 4 and 3 respectively lower than those implemented here. The difference is likely to be largely a consequence of the higher assumed photolysis rate for I$_2$O$_2$/I$_2$O$_3$/I$_2$O$_4$ in the Saiz-Lopez et al. study, and differences in model constraints and approaches to vertical mixing/ boundary layer height estimates.

6.3 NO$_x$ abundance and snowpack flux

The model is able to replicate the diurnal variation in NO$_x$ levels very well. The NO$_x$ lifetime is substantially reduced by the halogen reactions, as a consequence of deposition and heterogeneous loss of bromine and iodine nitrate. The halogen reactions lead to an increased NO-to-NO$_2$ conversion, dominated by the IO + NO and BrO + NO reactions for which the mean fluxes are factors of 1.16 and 0.96 times that through the NO + O$_3$ reaction. Overall the halogen chemistry results in an increase in NO-to-NO$_2$ conversion of a factor of 2.3 – clearly reflected in the observed NO and NO$_2$ levels (Fig. 4). The calculated mean NO$_x$ source strength of 3.7×10^8 molec cm^{-2} s^{-1} (case B2) is in reasonably good agreement with values measured during CHABLIS for specific 24-h periods of 1.7, 2.2 and 3.4×10^8 molec cm^{-2} s^{-1}

(Bauguitte et al., 2009), although the value reported here depends directly upon the assumed boundary layer height, and is in good agreement with explicit model simulations of snowpack nitrate photochemistry (Boxe and Saiz-Lopez, 2008). The NO$_x$ source strength is in excellent agreement with model-derived (3.2–4.2 × 10^8 molec cm^{-2} s^{-1}; Wang et al., 2008) and measured (3.9 × 10^8 molec cm^{-2} s^1; Oncley et al., 2004) NO$_x$ fluxes for South Pole, and is comparable with the NO$_x$ + HONO flux of 2.98 × 10^8 molec cm^{-2} s^{-1} measured at Summit, Greenland (Honrath et al., 2002). Our approach does not consider snowpack emissions of HONO (or rather, these are implicitly incorporated within the NO$_x$ flux). The calculated HONO mixing ratios (0.22 pmol/mol maximum; 0.1 pmol/mol diurnal mean) reflect the steady-state obtained from the gas phase OH + NO reaction source alone. These levels are much lower than observations of soluble nitrite reported using an aqueous stripping/ derivatisation/ colourimetry, with mean mixing ratios of 7 pmol/mol reported (Clemitshaw, 2006). In common with other studies, we cannot reconcile such levels with the observed NO$_x$ or HO$_x$ data to within even order-of-magnitude accuracy (Chen et al., 2004; Liao et al., 2006). If a proportion of our snowpack NO$_x$ source were in fact nitrous acid, this would also contribute to OH production, and would further worsen the model-measurement HO$_x$ comparison.

The calculated in situ chemical ozone destruction (mean rate 0.51 nmol/mol h^{-1}) is comparable with the value of 0.55 nmol/mol h^{-1} calculated by Saiz-Lopez et al. (2008), although for somewhat higher halogen monoxide mixing ratios (10 pmol/mol); in both cases iodine is found to dominate ozone destruction (although attribution is complicated by coupling through e.g. the IO + BrO reaction, and effects upon HO$_x$ and NO$_x$). These values would correspond to boundary layer ozone lifetimes of the order of 1 day, however no pronounced ozone depletion events were observed during the summertime CHABLIS measurement period (January/February 2005) considered here – rather ODEs have been historically apparent in the early spring (September–October) when halogen monoxide levels peak (Jones et al., 2008; Saiz-Lopez et al., 2007). We conclude that mixing of ozone from the free troposphere is necessary to offset the chemical loss (and deposition) – or that the iodine and bromine measured were released locally to the measurement site and insufficient time had elapsed for significant ozone loss, although this is unlikely given the short halogen lifetime (above) and uniformity of the Halley ice sheet location. Dilution from the free troposphere further implies that the calculated halogen and NO$_x$ production fluxes (Table 2) are lower limits.

6.4 Model – measurement OH and HO$_2$ overestimates

The model simulations substantially overestimated the observed OH and HO$_2$ levels. Potential reasons for the discrepancy include missing HO$_x$ sinks, overestimated HO$_x$ sources, errors in the model chemical scheme/ conditions, and errors in the observations. We consider each in turn below.

6.4.1 HO$_x$ sources and sinks

The principal OH sources are the photolysis of the hypohalous acids HOI and HOBr, whose steady-state concentrations depend upon the CH$_3$O$_2$-HO$_2$-HO$_x$ cycling simulated within the model. The principal overall HO$_x$ sources are photolysis of HCHO, photolysis of ozone, and the reaction of Br atoms with HCHO – if higher OVOCs are included, e.g. CH$_3$CHO, the Br + aldehyde HO$_x$ source becomes dominant, similar to conditions modelled above the Arctic boundary layer during ozone depletion events (Evans et al., 2003). As the measurements of ozone, humidity, HCHO and photolysis frequencies should be reliable, and OVOCs are if anything under-represented in the simulations, it seems unlikely that the HO$_x$ source has been significantly overestimated. The Br + HCHO source, constrained by the observed BrO levels, is the least certain parameter, but even setting this to zero would only reduce the overall modelled HO$_x$ source by approximately 31%, insufficient to account for the overestimate. As noted above, no snowpack HONO source is included in these simulations; addition of such a source (offsetting part of the NO$_x$ source) would worsen the model/observation discrepancy.

HO$_x$ sinks: in principle any measurement of ambient VOCs is likely to under-determine the true VOC population, and hence the true OH reactivity/ sink. Addition of unmeasured VOC species will increase the OH sink, and reduce modelled OH levels; however unlike polluted urban or forested environments where significant unmeasured OH reaction partners might reasonably be postulated (e.g. Lewis et al., 2000; Di Carlo et al., 2004) limited additional VOC sources are anticipated for the Antarctic coastal boundary layer. As a sensitivity test, the observed CH$_4$ and CO levels were doubled (CO and CH$_4$ represent 87% of the observed VOC sink), resulting in a reduction in peak OH levels of 31% with a concomitant 13% increase in HO$_2$. In previous studies, oxygenated VOCs (e.g. acetaldehyde, acetone) have been found to comprise a significant fraction of the total OH sink (Lewis et al., 2005). No OVOC measurements were attempted during CHABLIS (other than formaldehyde), however higher aldehydes have previously been observed in the Arctic boundary layer (Boudries et al., 2002; Houdier et al., 2002), and in conjunction with firn air observations suggest a net snowpack source to the overlying atmosphere (Guimbaud et al., 2002), potentially originating from the organic matter within snowpack (Domine et al., 2010). Laboratory experiments have shown similar production of acetaldehyde from South Pole snow (Grannas et al., 2004) and a similar mechanism might be expected to operate in other, related environments, i.e. at Halley. Acetaldehyde and other carbonyl species would affect the local radical chemistry, both through photolysis leading to radical production, and through

direct reaction with OH providing an additional OH sink (and peroxy radical source). For example, if acetaldehyde was present at the levels observed in the Arctic (29–459 pmol/mol during the 24-h daylight period – Boudries et al., 2002), the total OH sink would be increased by between 3 and 48%, giving a considerable reduction in the OH lifetime. This possibility was investigated using acetaldehyde as a proxy for all C$_2$ and higher OVOCs; CH$_3$CHO was added to the model following a diurnal profile (tracking j(NO$_2$) as reported by Boudries et al.), with a mean (24-h) mixing ratios of 166 pmol/mol. Such levels are considerably higher than those calculated to form in the course of gas-phase degradation of the measured NMHCs (maximum CH$_3$CHO mixing ratio 9.8 pmol/mol) implying a strong snowpack source if the chemical conditions are otherwise comparable. The simulated peak OH levels were reduced by 28%, while HO$_2$ rose by 5.9%. While agreement with observed HO$_x$ levels is improved, inclusion of CH$_3$CHO also affects the bromine chemistry – the model bromine source had to be increased by a factor of 5.3 relative to the iodine source change (the Br + CH$_3$CHO rate constant is a factor of 3.75 times larger than that for Br + O$_3$, and leads to HBr formation, effectively bromine loss on the timescale of these simulations/ boundary layer residence). In this scenario, the overall model bromine source required is much larger than that required for iodine (factor of 9.3, constrained by the observed XO levels), implying that either dissimilar iodine and bromine sources are present, and/or that aerosol (or snow surface) recycling of iodine is much more efficient than that for bromine – which is in keeping with our current understanding of these processes (von Glasow and Crutzen, 2007). Saiz-Lopez et al. (2008) have also shown that aerosol recycling reduces what would otherwise be pronounced vertical gradients in BrO at Halley, in keeping with observations in the Arctic (e.g. Avallone et al., 2003), although their simulations did not include surface fluxes of HCHO, CH$_3$CHO etc. which would also contribute to offsetting the bromine vertical profile. However, the Br + CH$_3$CHO reaction also causes deviations from the observed diurnal variation in BrO, introducing a substantial midday "dip" which is not observed (Fig. 1b; Saiz-Lopez et al., 2007a), indicating that either CH$_3$CHO levels must be below ca. 50 pmol/mol, and/or the levels do not follow a diurnal variation, and/or the bromine source follows an even stronger diurnal variation than that implemented here (which substantially worsens the model agreement for NO$_x$). These interactions may introduce the possibility of constraining bromine chemistry using OVOC observations, or vice versa, in future measurements. While inclusion of acetaldehyde, at levels and with the diurnal variation observed in similar environments, improves the model performance for OH, the reduction is not sufficient in isolation to explain the discrepancy from the observations, and significantly worsens the model performance for BrO. Hydrogen halides are another potential sink for OH, and hence HO$_x$: HBr formed from the reaction of bromine atoms with aldehydes, and HI potentially formed

from alternative channels of the IO + CH$_3$O$_2$ reaction. These species have lifetimes of a day/ several hours respectively so may potentially accumulate in the boundary layer – enhancing the impact of added aldehydes, and of changing the products for the IO + CH$_3$O$_2$ reaction (below).

6.4.2 Model conditions and chemistry

The sensitivity study identified a number of factors which could affect the modelled HO$_x$ levels, and over which there is significant uncertainty. Inspection of Fig. 7 indicates that two key factors are the kinetics/products of the IO + CH$_3$O$_2$ reaction, and the aerosol surface area. IO + CH$_3$O$_2$ competes with the peroxy-radical termination reactions, and with the CH$_3$O$_2$ + NO propagation step; laboratory measurements of the rate constant for this reaction vary by a factor of 30, from the "slow" results of Dillon et al. (2006), $k = 2 \times 10^{-12}$ molec^{-1}cm^3 s^{-1}, to the faster data from Bale et al. (2005) and Enami et al. (2007), both giving $k \sim (6$–$7) \times 10^{-11}$ molec^{-1} s^{-1} (298 K values). For typical peak IO levels observed of 6 pmol/mol, these correspond to pseudo-first-order rate constants for CH$_3$O$_2$ loss by reaction with IO of 3.2×10^{-4} and 0.01 s^{-1}, respectively, which may be compared with the equivalent rates for CH$_3$O$_2$ + NO and CH$_3$O$_2$ + HO$_2$ of 3.2×10^{-3} and 2.8×10^{-4} s^{-1} – i.e. the range of measured kinetics alters the CH$_3$O$_2$ fate dramatically, from reaction with NO dominating (radical propagation, ozone production) to reaction with IO being dominant (potentially more rapid radical propagation and ozone destruction). The trend in HO$_2$:OH ratios with NO$_x$ suggests that the role of the halogen species may be underestimated in the model at low levels of NO$_x$ – an increase in the CH$_3$O$_2$ + IO rate constant could account for this trend, as this reaction will be in competition with CH$_3$O$_2$ + NO. We preferred the Dillon et al. rate constant a priori as studies of complex radical-radical reactions typically suffer from secondary processes contributing to removal of the (monitored) reactants, correction for which is complex – consequently all other things being equal the lower rate constant was preferred. The products of the IO + CH$_3$O$_2$ reaction have not been confirmed; CH$_3$O + IOO might be anticipated by analogy with the NO reaction, while theoretical studies suggest that the CH$_3$O + OIO channel may also occur (Drougas and Kosmas, 2007) and formation of non-radical products (HCHO + HI + O$_2$) is thermodynamically feasible at $\Delta_r H$ (298 K) $= -207$ kJmol^{-1} (Bale et al., 2005) if mechanistically less likely given the transition state required. The identity of the products of the IO + CH$_3$O$_2$ reaction will exert a major impact upon the modelled iodine and HO$_x$ chemistry. As the CH$_3$O$_2$ + HO$_2$ reaction dominates the HO$_x$ sink (Fig. 6a), if modelled organic peroxy radical levels were underestimated, this could go some way to explaining the model – measurement discrepancy; however the additional halogen monoxide – RO$_2$ reactions shown to be of significance in this coastal Antarctic environment would seem to

indicate that organic peroxy radicals are a less important HO$_x$ sink than is the case in other low-NO$_x$ environments. Aerosol surface area was not measured during CHABLIS; the geographically closest measurements published were performed from a research ship in the adjacent Weddell Sea, some tens of km distant from the Halley V site, and a number of years earlier (Davison et al., 1996) obtained a value of 3×10^{-8} cm^{-1} for a subset of the full size distribution, comparable with our estimate of 10^{-7} cm^2 cm^{-3}. Local production and oxidation of DMS, accelerated by BrO (Read et al., 2008) and the new particle production which would result from sustained levels of 10's of pmol/mol of iodine monoxide (McFiggans et al., 2004) indicate that substantial local sources may exist. The MCM version 3.1 (as used here) does not include the minor channel of the HO$_2$ + NO reaction producing HNO$_3$ (Butskovaya et al., 2007); inclusion of this reaction following the expression recommended by IUPAC reduced HO$_x$ levels by 0.6%.

Chlorine chemistry could contribute to VOC oxidation and HO$_x$ radical production, and alter the partitioning of HO$_x$ and NO$_x$ species. No measurements of gas-phase chlorine species were made during CHABLIS, but some constraints may be obtained from VOC ratios. Using NMHC measurements obtained during CHABLIS, Read et al. (2006) estimated mean Cl atom concentrations from 1.7×10^3–3.4×10^4 cm^{-3} during local spring ozone depletion events, and a longer-term (springtime) value of 2.3×10^3 cm^{-3}. These absolute [Cl] levels are uncertain, being dependent upon assumed airmass processing times, and were derived for a different season to the measurements considered in the paper, but may be used to crudely constrain the potential effects of chlorine chemistry here. At the higher Cl level determined by Read et al. (3.4×10^4 cm^{-3}), considering only reaction with CH$_4$, Cl-initiated VOC oxidation would correspond to an RO$_2$ production rate of 9.6×10^4 molec cm^{-3} s^{-1}, respectively. This (effectively 24-h average) values may be compared with (24-h mean) calculated HO$_x$ production rates from O(^{1}D) + H$_2$O and HCHO photolysis of 9.72×10^4 and 1.25×10^5 molec cm^{-3} s^{-1}, respectively (Fig. 6b). It is therefore possible that Cl chemistry made a measureable contribution to radical production, worsening the model – measurement disagreement, if the elevated levels observed during Aug-Sept were also present during the summer. An argument against this is the pronounced seasonal cycle in sea salt aerosol observed at Halley (Wagenbach et al., 1998), which maximises during spring (when Read et al. performed their NMHC ratio analyses) and minimises in the summer (when the HO$_x$ observations were made), indicating that the actual Cl levels present are likely to be significantly lower than the values noted above. The second potential impact of chlorine chemistry arises through perturbations to HO$_x$ cycling analogous to the IO and BrO reactions discussed. Taking the higher [Cl] noted above (3.4×10^4 cm^{-3}) and the measured mean O$_3$ level to derive a ClO production rate, and consid-

ering ClO removal by reaction with itself, IO, BrO, HO$_2$, NO and NO$_2$, steady-state ClO concentrations of 8.3×10^6 molecules cm^{-3} are obtained (ClO removal dominated by the well-constrained ClO + NO reaction). At a typical peak HO$_2$ level of 2 nmolmol^{-1}, the flux through the HO$_2$ + ClO reaction is 3×10^{-4} nmolmol^{-1} h^{-1}, which is approximately a factor of 130 less than the main OH production and HO$_2$ removal rates (Fig. 6b). It is therefore unlikely that chlorine chemistry is having a significant impact upon either the HO$_x$ production or partitioning in this environment.

6.4.3 Observations

The fundamental observations which this analysis is based upon are the measurements of NO$_x$, the halogen monoxide species, VOCs (CH$_4$, CO, HCHO), O$_3$, H$_2$O, photolysis frequencies and OH/ HO$_2$. The NO chemiluminescence measurement should be robust – the NO$_x$ levels are low, but are not in the single-ppt range which become marginal for such instruments. The observed halogen monoxide levels are direct absorption measurements, whose systematic error is limited by the literature absorption cross sections, of the order of 10–15%. The DOAS beam path was entirely uniform over the ice sheet, so heterogeneity should not be an issue. The number of observations over the measurement period is limited (Fig. 1) so the assumption that these are representative may be incorrect (although the data available do bracket the time period). The DOAS BrO observations in particular are variable, and the observed high variability in HCHO indicates this variability may be typical of the summer measurement period, as reaction with Br accounts for ca. 45% of the chemical HCHO loss rate (Salmon et al., 2008). A sensitivity test in which the source strengths were adjusted to (arbitrarily) halve the IO and BrO levels resulted in changes to OH and HO$_2$ of $+18$ and -32%, respectively, but also resulted in the model failing to capture the observed NO and NO$_2$ diurnal profiles (Fig. 4), indicating that the observed XO levels are in fact representative. The HCHO measurements were a factor of 3–4 times lower than those observed at Neumayer station previously (Reidel et al., 1999), but it is not clear why the levels should be dramatically different from those at Halley – if anything, higher halogen levels might be anticipated for the coastal Neumayer site resulting in reduced HCHO (Salmon et al., 2008). Increasing HCHO by a factor of 4 increased simulated OH by 40 % and doubled the modelled HO$_2$. Measurements of O$_3$ and H$_2$O were performed by well-established methods using calibrated instruments, and would have to be greatly in error to account for the model-measurement discrepancy. Photolysis frequencies were derived from a calibrated spectral radiometer, and the j(O^{1}D) data obtained were in agreement with those measured by an adjacent filter radiometer (Bloss et al., 2007).

An obvious explanation for the model – measurement HO$_x$ discrepancy is the accuracy of the HO$_x$ observations. The measurement approach is explained in detail in Bloss et

al. (2007), which includes a derivation of the estimated measurement uncertainty (27%, 1 standard deviation, combined known systematic factors and precision), and the interference tests performed during the campaign. The model – measurement discrepancy observed here (Table 3) is substantially greater than this, indicating that either there are unidentified problems with the HO$_x$ measurement, or with the other observations and model approximations adopted. The instrument performance, as assessed by the calibration factor, was approximately constant over the duration of the campaign, and the calibration conditions (temperature, humidity) bracketed the ambient conditions encountered. We are unable to identify any specific problems with the HO$_x$ measurements, which would not also be apparent in other environments, where the instrument (and other analogous systems) have performed well (e.g. Bloss et al., 2004). A recent blind intercomparison of OH and HO$_2$ measurements (Schlosser et al., 2009; Fuchs et al., 2010), between instruments very similar to that used here, has shown good agreement for OH (relative range up to 1.13) but substantial variability for HO$_2$ (relative range up to 1.45) for chamber experiments where homogeneity of sampled air is guaranteed. The latter value is somewhat larger than the known measurement uncertainty for the HO$_x$ data discussed here would indicate, and may indicate that additional sources of measurement error are present – but would not in isolation account for the model – measurement discrepancy found here. We cannot identify any cause for such a significant measurement problem, hence also consider other potential explanations for the discrepancy considering the known uncertainties within the chemical and physical parameters – additional unknown uncertainties may of course also be present, in both model and measurements.

In a final simulation, as a test case for the potential combined impact of model conditions and chemical scheme, the fast kinetics and non-radical products for IO + CH$_3$O$_2$ were adopted and the aerosol surface area increased to 3×10^{-7} cm^{-2} cm^{-3} – this simulation is shown as case C on Figs. 2 and 6a; modelled OH and HO$_2$ were reduced on average by 46% and 37%, respectively – still a substantial model overestimate but indicative of the variation accessible within the uncertainty of the constraining parameters. Inclusion of additional OH sinks – for example modest OVOC (CH$_3$CHO) would further improve the model performance for OH, but at the expense of worsening performance for BrO and hence for NO$_x$.

Analyses of HO$_x$ measurements in related environments have also encountered difficulty in reconciling observations with model predictions. Model analyses of OH and HO$_2$ + RO$_2$ data measured at Summit Greenland were able to replicate the observed peroxy radical levels, but substantially *under*estimated observed OH levels (Sjostedt et al., 2007; Chen et al., 2007). Sjostedt et al. suggested that (unmeasured) halogen chemistry may provide an additional RO$_2$/HO$_2$ to OH conversion mechanism, accounting

for the discrepancy – this suggestion is consistent with our results, where IO and BrO have been shown to overwhelmingly dominate HO$_2$-to-OH conversion. Sjostedt et al. reported a wind-speed dependence to the modelled:observed OH ratio – we found no such correlation between wind-speed and model:measured OH or HO$_2$ ratios, possibly supporting the alternative explanation of a windspeed-dependent measurement artefact at Summit. In their model analysis of South Pole HO$_x$ data recorded during ISACAT 2000, Chen et al. (2004) found a substantial model overestimate of OH and HO$_2$ levels when measured HONO was used as a constraint; excluding HONO data resulted in a modest model overestimate of the observed OH and HO$_2$ levels, by 20–50%. Chen et al. reported a significant dependence of the model OH overestimate upon NO levels, while in this work the model:measured OH ratio was independent of NO$_x$, but some NO$_x$ dependence was apparent for HO$_2$, which we tentatively attribute to a local wind direction dependence of the actual halogen levels, manifested through changed competition between NO and IO/BrO in driving HO$_x$ cycling. The NO$_x$ levels at Halley were much lower than those at South Pole, likely a result of the low boundary layer height in the latter case as the surface NO$_x$ fluxes derived are very similar, and consequently the loss/recycling of NO$_x$ reservoirs such as PNA and HNO$_3$, critical in the South Pole environment, were less important at Halley. The role of the halogen species (plus lower NO$_x$ levels compared to the case of South Pole) is the principal difference between the Halley data and that from South Pole and Summit, and as has been demonstrated above the identified uncertainties over the physical conditions during the CHABLIS campaign, and within the halogen chemical kinetics and photochemistry, can bring the modelled HO$_x$ levels close to those observed.

Comparing the derived HO$_x$ sources and sinks between the "polar" boundary layer measurements at South Pole, Halley and Summit reveals significant differences between these locations: At both South Pole and Summit, HO$_x$ production was found to be dominated by photolysis of snowpack-derived HCHO and H$_2$O$_2$, and O(^{1}D) + H$_2$O, while at Halley, the analysis presented here identifies a major role for bromine-initiated oxidation of aldehydes, accounting for about 30% of the measured HO$_x$ source strength, potentially more if higher aldehydes are also present. HO$_x$ sinks were dominated by HO$_2$ + HO$_2$ at Summit, and by NO$_x$-related processes such as PNA and HNO$_3$ formation and removal, together with OH + HO$_2$ reaction, in the South Pole case, while for Halley the major terms were found to be HO$_2$ + CH$_3$O$_2$ and HO$_2$ + HO$_2$, with halogen-mediated processes accounting for ca. 40% of the HO$_x$ loss under the base case model scenario, with this fraction potentially increasing dependent upon assumptions within the iodine chemical scheme. At South Pole, elevated NO$_x$ lead to local chemical ozone production at rates of 1–6 nmol/mol day^{-1} (Chen et al., 2004; Crawford et al., 2001), while at Halley the halogens result in net local chemical ozone destruction at rates

equivalent to 8–12 nmol/mol day^{-1}. The transition between these environments will be determined by the geographic extent of influence of the halogen species – satellite observations indicate these are associated with sea ice cover (Saiz-Lopez et al., 2007b; Schönhardt et al., 2008), indicating that conditions similar to those considered here (Halley) may be representative of a substantial area of the Southern Hemisphere boundary layer.

7   Conclusions

A detailed photochemical model has been used to simulate coupled HO_x, NO_x and halogen chemistry based upon observations performed in the coastal Antarctic boundary layer during the CHABLIS campaign at Halley research station.

The model NO_x source required to replicate observed NO and NO_2 levels was in very good agreement with that directly measured during CHABLIS, and with values obtained elsewhere, if the substantial HONO flux implied by observations of soluble nitrite were discounted. The model was able to replicate the diurnal variation in NO and NO_2 concentrations, using a simple source expression which assumed the net snowpack NO_x production was proportional to the photolysis frequency for the nitrate anion. The halogen species increase the NO_2:NO ratio, and substantially reduce the NO_x lifetime through heterogeneous loss of the halogen nitrates.

The principal sources of HO_x radicals were the photolysis and bromine-initiated oxidation of HCHO, together with $O(^1D) + H_2O$. The main sinks for HO_x were peroxy radical self- and cross-reactions, with the sum of all halogen-mediated HO_x loss processes accounting for 40 % of the total sink. Reactions with the halogen monoxides dominated CH_3O_2-HO_2-OH interconversion, with associated ozone destruction, at rates of up to 0.3–0.5 nmol/mol h^{-1}, in place of the ozone production which is associated with the analogous NO reactions. Iodine chemistry accelerates production of formaldehyde, through the $CH_3O_2 + IO$ reaction, while reaction of bromine atoms with HCHO and higher aldehydes comprises a major HO_x source, both processes linking the I, Br and HO_x chemical families. This coupling alters oxidant levels, represents a further atmospheric impact of halogen chemistry in polar boundary layer environments.

The base case model significantly overpredicted the observed levels of OH and HO_2. The model overestimate is substantially greater than the known HO_x measurement/calibration uncertainty, and greater than the variability which has been found between OH and HO_2 measurements during recent intercomparison exercises; nonetheless unidentified HO_x measurement error could account for the discrepancy with the model. Alternatively, known uncertainties within the model assumptions and chemical scheme can resolve much of the discrepancy: agreement could be improved with variations in physical parameters (boundary layer height and aerosol surface area, which were not measured) and by

modifying the base case halogen chemical scheme, within the uncertainty of the available laboratory studies. The model could also be brought into better agreement with the observations through the addition of (unmeasured) chemical species, in particular OVOCs such as acetaldehyde, but at levels comparable with those observed elsewhere the predicted HO_x levels were still higher than those observed, while agreement for BrO was worsened. As the $CH_3O_2 + HO_2$ reaction was a dominant HO_x sink, a model underestimate of organic peroxy radical levels could contribute to the discrepancy with observations; measurement of atmospheric RO_2 abundance would assess this possibility. The analysis highlights the need for observations of physical parameters such as aerosol surface area and boundary layer structure to constrain such calculations, and the dependence of simulated radical levels and ozone loss rates upon a number of uncertain kinetic and photochemical parameters for iodine species, in particular relating to the fates of iodine nitrate and higher iodine oxides, and halogen oxide – peroxy radical reactions.

Supplementary material
related to this article is available online at:
http://www.atmos-chem-phys.net/10/10187/2010/
acp-10-10187-2010-supplement.pdf.

References

Allan, B. J. and Plane, J. M. C.: A Study of the Recombination of IO with NO_2 and the Stability of INO_3: Implications for the Atmospheric Chemistry of Iodine, J. Phys. Chem. A, 106, 8634–8641, 2002.

Aranda, A., Le Bras, G., La Verdet, G., and Poulet, G.: The $BrO + CH_3O_2$ reaction: Kinetics and role in the atmospheric ozone budget, Geophys. Res. Lett., 24, 2745–2748, 1997.

Atkinson, R., Baulch, D. L., Cox, R. A., Crowley, J. N., Hampson, R. F., Hynes, R. G., Jenkin, M. E., Rossi, M. J., and Troe, J.: Evaluated kinetic and photochemical data for atmospheric chemistry: Volume III gas phase reactions of inorganic halogens, Atmos. Chem. Phys., 7, 981–1191, doi:10.5194/acp-7-981-2007, 2007.

Avallone, L. M., Toohey, D. W., Fortin, T. J., McKinney, K. A., and Fuentes, J. D.: In situ measurements of bromine oxide at two

high-latitude boundary layer sites: Implications of variability, J. Geophys. Res., 108, 4089, doi:10.1029/2002JD002843, 2003.

Bale, C. S. E., Canosa-Mas, C. E., Shallcross, D. E., and Wayne, R. P.: A discharge-flow study of the kinetics of the reactions of IO with CH$_3$O$_2$ and CF$_3$O$_2$, Phys. Chem. Chem. Phys., 7, 2164–2172, 2005.

Bauguitte, S. J.-B., Bloss, W. J., Evans, M. J., Salmon, R. A., Anderson, P. S., Jones, A. E., Lee, J. D., Saiz-Lopez, A., Roscoe, H. K., Wolff, E. W., and Plane, J. M. C.: Summertime NO$_x$ measurements during the CHABLIS campaign: can source and sink estimates unravel observed diurnal cycles?, Atmos. Chem. Phys. Discuss., 9, 20371–20406, doi:10.5194/acpd-9-20371-2009, 2009.

Braban, C. F., Adams, J. W., Rodriguez, D., Cox, R. A., Crowley, J. N., and Schuster, G.: Heterogeneous reactions of HOI, ICl and IBr on sea salt and sea salt proxies, Phys. Chem. Chem. Phys., 9, 3136–3148, 2007.

Bloss, W. J., Rowley, D. W., Cox, R. A., and Jones, R. L.: Kinetics and Products of the IO Self-Reaction, J. Phys. Chem. A, 105, 7840–7854, 2001.

Bloss, W. J., Lee, J. D., Bloss, C., Heard, D. E., Pilling, M. J., Wirtz, K., Martin-Reviejo, M., and Siese, M.: Validation of the calibration of a laser-induced fluorescence instrument for the measurement of OH radicals in the atmosphere, Atmos. Chem. Phys., 4, 571–583, doi:10.5194/acp-4-571-2004, 2004.

Bloss, W. J., Lee, J. D., Johnson, G. P., Heard, D. E., Sommariva, R., Plane, J. M. C., Saiz-Lopez, A., McFiggans, G., Coe, H., Flynn, M., Williams, P., Rickard, A., and Fleming, Z.: Impact of Halogen Monoxide Chemistry upon Boundary Layer OH and HO$_2$ concentrations at a Coastal Site, Geophys. Res. Lett., 32, L068414, doi:10.1029/2004GL022084, 2005.

Bloss, W. J., Lee, J. D., Heard, D. E., Salmon, R. A., Bauguitte, S. J.-B., Roscoe, H. K., and Jones, A. E.: Observations of OH and HO2 radicals in coastal Antarctica, Atmos. Chem. Phys., 7, 4171–4185, doi:10.5194/acp-7-4171-2007, 2007.

Boxe, C. S. and Saiz-Lopez, A.: Multiphase modeling of nitrate photochemistry in the quasi-liquid layer (QLL): implications for NOx release from the Arctic and coastal Antarctic snowpack, Atmos. Chem. Phys., 8, 4855–4864, doi:10.5194/acp-8-4855-2008, 2008.

Burkholder, J. B., Curtius, J., Ravishankara, A. R., and Lovejoy, E. R.: Laboratory studies of the homogeneous nucleation of iodine oxides, Atmos. Chem. Phys., 4, 19–34, doi:10.5194/acp-4-19-2004, 2004.

Butkovskaya, N., Kukui, A. and Le Bras, G.: HNO$_3$ Forming Channel of the HO$_2$ + NO Reaction as a Function of Pressure and Temperature in the Ranges of 72–600 Torr and 223–323 K, J. Phys. Chem. A, 111, 9047–9053, 2007.

Carslaw, N., Creasey, D. J., Heard, D. E., Lewis, A. C., McQuaid, J. B., Pilling, M. J., Monks, P. S., Bandy, B. J., and Penkett, S. A.: Modeling OH, HO$_2$ and RO$_2$ radicals in the marine boundary layer 1. Model construction and comparison with field measurements, J. Geophys. Res., 104, 30241–30255, 1999.

Chen, G., Davis, D., Crawford, J., Nowak, J.B., Eisele, F., Mauldin III, R. L., Tanner, D., Buhr, M., Shetter, R., Lefer, B., Arimoto, R., Hogan, A., and Blake, D.: An Investigation of South Pole HO$_x$ Chemistry: Comparison of Model Results with ISCAT Observations, Geophys. Res. Lett., 28, 3633–3636, 2001.

Chen, G., Davis, D., Crawford, J., Hutterli, L.M., Huey, L.G., Slusher, D., Mauldin, L., Eisele, F., Tanner, D., Dibb, J., Buhr, M., McConnell, J., Lefer, B., Shetter, R., Blake, D., Song, C.H., Lombardo, K., and Arnoldy, J.: A reassessment of HO$_x$ South Pole chemistry based on observations recorded during ISCAT 2000, Atmos. Environ., 38, 5451–5461, 2004.

Chen, G., Huey, L. G., Crawford, J. H., Olson, J. R., Hutterli, M. A., Sjostedt, S., Tanner, D., Dibb, J., Lefer, B., Blake, N, Davis, D., and Stohl, A.: An assessment of the polar HO$_x$ photochemical budget based on 2003 Summit Greenland field observations, Atmos. Environ., 41, 7806–7820, 2007.

Clemitshaw, K. C., Coupling between the Tropospheric Photochemistry of Nitrous Acid (HONO) and Nitric Acid (HNO$_3$), Environ. Chem., 3, 31–34, 2006.

Cotter, E. S. N., Jones, A. E., Wolff, E. W., and Bauguitte, S. J.-B.: What controls photochemical NO and NO2 production from Antarctic snow ? Laboratory investigation assessing the wavelength and temperature dependence. J. Geophys. Res. 108, doi:10.1029/2002JD002602, 2003.

Cox, R. A., Bloss, W. J., Jones, R. L., and Rowley, D. M.: OIO and the Atmospheric Cycle of Iodine, Geophys. Res. Lett., 26, 1857–1860, 1999

Crawford, J. H., Davis, D. D., Chen, G., Buhr, M., Oltmans, S., Weller, R., Mauldin, L., Eisele, F., Shetter, R., Lefer, B., Arimoto, R., and Hogan, A.: Evidence for photochemical production of ozone at the South Pole surface, Geophys. Res. Lett., 28, 3641–3644, 2001.

Davis, D., Nowak. J. B., Chen, G., Buhr, M., Arimoto, R., Hogan, A., Eisele, F., Mauldin, L., Tanner, D., Shetter, R., Lefer, B., and McMurry, P.: Unexpected High Levels of NO Observed at South Pole, Geophys. Res. Lett., 28, 3625–3628, 2001.

Davison, B., Hewitt, C. N., O'Dowd, C., Lowe, J. A., Smith, M. H., Schwikowski, M., Baltensperger, U. and Harrison, R. M.: Dimethyl sulphide, methane sulphonic acid and the physiochemical aerosol properties in Atlantic air from the United Kingdom to Halley Bay, J. Geophys. Res., 101, 22855–22867, 1996.

Domine, F., Houdier, S., Taillandier, A.-S., and Simpson, W. R.: Acetaldehyde in the Alaskan subarctic snowpack, Atmos. Chem. Phys., 10, 919–929, doi:10.5194/acp-10-919-2010, 2010.

Di Carlo, P., Brune, W. H., Martinez, M., Harder, H., Lesher, R., Ren, X., Thornberry, T., Carroll, M. A., Young, V., Shepson, P. B., Riemer, D., Apel, E., and Campbell, C.: Missing OH Reactivity in a Forest: Evidence for Unknown Reactive Biogenic VOCs, Science, 304, 722–725, 2004.

Dillon, T. J., Tucceri, M. E., and Crowley, J. N.: Laser induced fluorescence studies of iodine oxide chemistry, Phys. Chem. Chem. Phys., 8, 5185–5198, 2006.

Dillon, T. J., Tucceri, M. E., Sander, R., and J. N. Crowley, LIF Studies of Iodine Oxide Chemistry Part 3. Reactions IO + NO$_3$ → OIO + NO$_2$, I + NO$_3$ → IO + NO$_2$ and CH$_2$I + O$_2$ → (products): implications for the chemistry of the marine atmosphere at night, Phys. Chem. Chem. Phys., 10, 1540–1554, 2008.

Drougas, E. and Kosmas, A. M.: Ab Intitio Characterization of (CH$_3$IO$_3$) Isomers and the CH$_3$O$_2$ + IO Reaction Pathways, J. Phys. Chem. A, 111, 3402–3408, 2007.

Eisele, F., Davis, D. D., Helming, D., Oltmans, S. J., Neff, W., Huey, G., Tanner, D., Chen, G., Crawford, J., Arimoto, R., Buhr, M., Mauldin, L., Hutterli, M., Dibb, J., Blake, D., Brooks, S. B., Johnson, B., Roberts, J. M., Wang, Y., Tan, D. and Flocke, F.:

Antarctic Tropospheric Chemistry Investigation (ANTCI) 2003 overview, Atmos. Environ., 42, 2749–2761, 2008.

Enami, S., Yamanaka, T., Hashimoto, S., Kawasaki, M., Nakano, Y., and Ishiwata, T.: Kinetic Study of IO Radical with RO_2 ($R = CH_3$, C_2H_5, and CF_3) Using Cavity Rind-Down Spectroscopy, J. Phys. Chem. A, 110, 9861–9866, 2006.

Enami, S., Yamanaka, T., Nakayama, T., Hashimoto, S., Kawasaki, M., Shallcross, D. E., Nakano, Y., and Ishiwata, T.: A Gas-Phase Kinetic Study of the Reaction between Bromine Monoxide and Methylperoxy Radicals at Atmospheric Temperatures, J. Phys. Chem. A, 111, 3342–3348, 2007.

Evans, M. J., Jacob, D. J., Altlas, E., Cantrell, C. A., Eisele, F., Flocke, F., Fried, A., Mauldin, R. L., Ridley, B. A., Wert, B., Talbot, R., Blake, D., Heikes, B., Snow, J., Walega, J., Weinheimer, A. J., and Dibb, J.: Coupled evolution of BrO_x-ClO_x-HO_x-NO_x chemistry during bromine catalyzed ozone depletion events in the arctic boundary layer, J. Geophys. Res., 108, 8368, doi:10.1029/2002JD002732, 2003.

Fuchs, H., Brauers, T., Dorn, H.-P., Harder, H., Hässler, R., Hofzumahaus, A., Holland, F., Kanaya, Y., Kajii, Y., Kubistin, D., Lou, S., Martinez, M., Miyamoto, K., Nishida, S., Rudolf, M., Schlosser, E., Wahner, A., Yoshino, A., and Schurath, U.: Technical Note: Formal blind intercomparison of HO_2 measurements in the atmosphere simulation chamber SAPHIR during the HOxComp campaign, Atmos. Chem. Phys. Discuss., 10, 21189–21235, doi:10.5194/acpd-10-21189-2010, 2010.

Gómez Martin, J. C., Spietz, P., and Burrows, J. P.: Kinetic and Mechanistic Studies of the I_2/O_3 Photochemistry, J. Phys. Chem. A, 111, 306–320, 2007.

Gómez-Martin, J. C., Ashworth, S. H., Mahajan, A. S., and Plane, J. M. C.: Photochemistry of OIO: Laboratory study and atmospheric implications, Geophys. Res. Lett., 36, L09802, doi:10.1029/2009GL037642, 2009.

Grannas, A., M., Shepson, P. B., Guimbaud, C., Sumner, A. L., Albert, M., Simpson, W., Domine, F., Boudries, H., Bottenheim, J., Beine, H. J., Honrath, R., and Zhou, X.: A study of photochemical and physical processes affecting carbonyl compounds in the Arctic atmospheric boundary layer, Atmos. Environ., 36, 2733–2742, 2002.

Grannas, A. M., Jones, A. E., Dibb, J., Ammann, M., Anastasio, C., Beine, H. J., Bergin, M., Bottenheim, J., Boxe, C. S., Carver, G., Chen, G., Crawford, J. H., Dominé, F., Frey, M. M., Guzmán, M. I., Heard, D. E., Helmig, D., Hoffmann, M. R., Honrath, R. E., Huey, L. G., Hutterli, M., Jacobi, H. W., Klán, P., Lefer, B., McConnell, J., Plane, J., Sander, R., Savarino, J., Shepson, P. B., Simpson, W. R., Sodeau, J. R., von Glasow, R., Weller, R., Wolff, E. W., and Zhu, T.: An overview of snow photochemistry: evidence, mechanisms and impacts, Atmos. Chem. Phys., 7, 4329–4373, doi:10.5194/acp-7-4329-2007, 2007.

Honrath, R. E., Peterson, M. C., Guo, S., Dibb, J. E., Shepson, P. B., and Campbell, B.: Evidence of NO_x production within or upon ice particles in the Greenland snowpack, Geophys. Res. Lett., 26, 695–698, 1999.

Honrath, R. E., Lu, Y., Peterson, M. C., Dibb, J. E., Arsenault, M. A., Cullen, N. J., and Steffen, K.: Vertical fluxes of NO_x, HONO, and HNO_3 above the snowpack at Summit, Greenland, Atmos. Environ., 36, 2629–2640, 2002.

Houdier, A., Perrier, S., Dominé, F., Cabanes, A., Legagneux, L., Grannas, A. M., Guimbaud, G., Shepson, P. B., Boudries, H.,

and Bottenheim, J. W.: Acetaldeyhde and acetone in the Arctic snowpack during the ALERT2000 cmapgin. Snowpack composition, incorporation processes and atmospheric impact. Atmos. Environ., 36, 2609–2618, 2002.

Hough, A. M.: The calculation of photolysis rates for use in global tropospheric modelling studies, AERE Report R-13259, HMSO, London, UK, 1988.

Hutterli, M. A., Röthlisberger, R., and Bales, R. C.: Atmosphere-to-snow-to-firn transfer studies of HCHO at Summit, Greenland, Geophys. Res. Lett., 26, 1691–1694, 1999.

Ingham, T., Cameron, M., and Crowley, J. N.: Photodissociation of IO (355 nm) and OIO (532 nm): quantum Yields for $O(^3P)$ and $I(^2P_J)$ Production, J. Phys. Chem. A, 104, 8001–8010, 2000.

Jacob, D. J.: Heterogeneous chemistry and tropsopheric ozone, Atmos. Environ. 34, 2131–2159, 2000.

Jefferson, A., Tanner, D. J., Eisele, F. L., Davis, D. D., Chen, G., Crawford, J., Huey, J. W., Torres, A. L. and Berresheim, H.: OH Photochemistry and methane sulphonic acid formation in the coastal Antarctic boundary layer, J. Geophys. Res., 103, 1647–1656, 1998.

Jones, A. E., Weller, R., Wolff, E. W., and Jacobi, H.-W.: Speciation and Rate of Photochemical NO and NO_2 Production in Antarctic Snow, Geophys. Res. Lett., 27, 345–348, 2000.

Jones, A. E., Wolff, E. W., Ames, D., Bauguitte, S. J.-B., Clemitshaw, K. C., Fleming, Z., Mills, G. P., Saiz-Lopez, A., Salmon, R. A., Sturges, W. T., and Worton, D. R.: The multi-seasonal NO_y budget in coastal Antarctica and its link with surface snow and ice core nitrate: results from the CHABLIS campaign, Atmos. Chem. Phys. Discuss., 7, 4127–4163, doi:10.5194/acpd-7-4127-2007, 2007.

Jones, A. E., Wolff, E. W., Salmon, R. A., Bauguitte, S. J.-B., Roscoe, H. K., Anderson, P. S., Ames, D., Clemitshaw, K. C., Fleming, Z. L., Bloss, W. J., Heard, D. E., Lee, J. D., Read, K. A., Hamer, P., Shallcross, D. E., Jackson, A., Walker, S., Lewis, A. C., Mills, G. P., Plane, J. M. C., Saiz-Lopez, A., Sturges, W. T., and Worton, D. R.: Chemistry of the antarctic boundary layer and the interface with snow: an overview of the CHABLIS campaign, Atmos. Chem. Phys. Discuss., 8, 5137–5181, doi:10.5194/acpd-8-5137-2008, 2008.

Joseph, D. M., Ashworth, S. H., and Plane, J. M. C.: The absorption cross-section and photochemistry of OIO, J. Photochem. Photobiol. A: Chemistry, 176, 68–77, 2005.

Joseph, D. M., Ashworth, S. H., and Plane, J. M. C.: On the photochemistry of $IONO_2$: absorption cross section (240–370 nm) and photolysis product yields at 248 nm, Phys. Chem. Chem. Phys., 9, 5599–5607, 2007.

Kaltsoyannis, N. and Plane, J. M. C.: Quantum chemical calculations on a selection of iodine containing species (IO, OIO, INO_3, $(IO)_2$, I_2O_3, I_2O_4 and I_2O_5) of importance in the atmosphere, Phys. Chem. Chem. Phys., 10, 1723–1733, 2008.

Kanaya, Y., Sadanaga, Y., Nakumura, K., and Akimoto, H.: Behavior of OH and HO_2 radicals during the Observations at a Remote Island of Okinawa (ORION99) field campaign: 1. Observation using a laser-induced fluorescence instrument, J. Geophys. Res., 106, 24197–2428, 2001.

König-Langlo, G., King, J., and Pettre, P.: Climatology of the three coastal Antarctic stations Dumont d'Urville, Neumayer and Halley, J. Geophys. Res., 103, 10935–10946, 1998.

Legrand, M., and Mayewski, P.: Glaciochemistry of Polar Ice

Cores: A Review, Rev. Geophys., 35, 219–243, 1997.

Lewis, A. C., Carslaw, N., Marriott, P. J., Kinghorn, R. M., Morrison, P., Lee, A. L., Bartle, K. D., and Pilling, M. J.: A larger pool of ozone-forming carbon compounds in urban atmospheres, Nature, 405, 778–781, 2000.

Lewis, A. C., Hopkins, J. R., Carpenter, L. J., Stanton, J., Read, K. A., and Pilling, M. J.: Sources and sinks of acetone, methanol, and acetaldehyde in North Atlantic marine air, Atmos. Chem. Phys., 5, 1963–1974, doi:10.5194/acp-5-1963-2005, 2005.

Liao, W., Case, A. T., Mastromarino, J., Tan, D. and Dibb, J. E.: Observations of HONO by laser-induced fluorescence at the South Pole during ANTCI 2003, Geophys. Res. Lett. 33, L09810, doi:10.1029/2005GL025470, 2006.

Madronich, S., and Flocke, S.: The role of solar radiation in atmospheric chemistry, in Handbook of Environmental Chemistry, edited by: Boule, P., Springer Verlag, Heidelberg, Germany, 1–26, 1998.

Mauldin, R., Kosciuch, E., Eisele, F., Huey, G., Tanner, D., Sjostedt, S., Blake, D., Chen, G., Crawford, J., and Davis, D.: South Pole Antarctica observations and modeling results: New insights on HO$_x$ radical and sulfur chemistry, Atmos. Environ., 44, 572–581, 2010.

Maricq, M. M., Szente, J. J., Kaiser, E. W., and Shi, J.: Reaction of Chlorine Atoms with Methyl and Ethylperoxy Radicals, J. Phys. Chem., 98, 2083–2089, 1994.

Mauldin III, R. L., Eisele, F. L., Tanner, D. J., Kosciuch, E., Shetter, R., Lefer, B., Hall, S. R., Nowak, J. B., Buhr, M., Chen, G., Wang, P., and Davis, D.: Measurements of OH, H$_2$SO$_4$, and MSA at the South Pole during ISCAT, Geophys. Res. Lett., 28, 3629–3632, 2001.

Mauldin III, R.L., Kosciuch, E., Henry, B., Eisele, F.L., Shetter, R., Lefer, B., Chen, G., Davis, D., Huey, G., and Tanner, D.: Measurements of OH, HO$_2$ + RO$_2$, H$_2$SO$_4$ and MSA at the South Pole during ISCAT 2000, Atmos. Environ., 38, 5423–5437, 2004.

McFiggans, G., Plane, J. M. C., Allan, B. J., Carpenter, L. J., Coe, H., and O'Dowd, C.: A modelling study of iodine chemistry in the marine boundary layer, J. Geophys. Res., 105, 14371–14385, 2000.

McFiggans, G., Coe, H., Burgess, R., Allan, J., Cubison, M., Alfarra, M. R., Saunders, R., Saiz-Lopez, A., Plane, J. M. C., Wevill, D., Carpenter, L., Rickard, A. R., and Monks, P. S.: Direct evidence for coastal iodine particles from Laminaria macroalgae linkage to emissions of molecular iodine, Atmos. Chem. Phys., 4, 701–713, doi:10.5194/acp-4-701-2004, 2004.

Mössinger, J. C., and Cox, R. A.: Heterogeneous reaction of HOI with sodium halide salts, J. Phys. Chem., A, 105, 5165–5177, 2001.

Mössinger, J. C., Rowley, D. M., and Cox, R. A.: The UV-visible absorption cross-sections of IONO$_2$, Atmos. Chem. Phys., 2, 227–234, doi:10.5194/acp-2-227-2002, 2002.

Oncley, S. P., Buhr, M., Lenschow, D. H., Davis, D., and Semmera, S. R.: Observations of summertime NO fluxes and boundary-layer height at the South Pole during ISCAT 2000 using scalar similarity, Atmos. Environ., 38, 5389–5398, 2004.

Orlando, J. J. and Tyndall, G. S.: Rate Coefficients for the Thermal Decomposition of BrONO$_2$ and the Heat of Formation of BrONO$_2$, J. Phys. Chem., 100, 19398–19405, 1996.

Plane, J. M. C., Joseph, D. M., Allan, B. J., Ashworth, S. H., and Francisco, J. S.: An Experimental and Theoretical Study of the Reactions OIO + NO and OIO + OH, J. Phys. Chem., 110, 93–100, 2006.

Rowley, D. M., Bloss, W. J., Cox, R. A., and Jones, R. L.: Kinetics and Products of the IO + BrO Reaction, J. Phys. Chem. A, 105, 7855–7864, 2001.

Read, K. A., Lewis, A. C., Salmon, R. A., Jones, A. E. and Bauguitte, S.: OH and halogen atom influence on the variability of non-methane hydrocarbons in the Antarctic Boundary Layer, Tellus B, 59, 22–38, 2007.

Read, K. A., Lewis, A. C., Bauguitte, S., Rankin, A. M., Salmon, R. A., Wolff, E. W., Saiz-Lopez, A., Bloss, W. J., Heard, D. E., Lee, J. D., and Plane, J. M. C.: DMS and MSA measurements in the Antarctic Boundary Layer: impact of BrO on MSA production, Atmos. Chem. Phys., 8, 2985–2997, doi:10.5194/acp-8-2985-2008, 2008.

Ren, X., Harder, H., Martinez, M., Lesher, R. L., Oliger, A., Shirley, T., Adams, J., Simpas, J. B., and Brune, W. H.: HOx concentrations and OH reactivity observations during the PMTACS-NY 2001 campaign in New York City, Atmos. Environ., 37, 3627–3637, 2003.

Riedel, K., Weller, R., and Schrems, O.: Variability of formaldehyde in the Antarctic troposphere, Phys. Chem. Chem. Phys., 1, 5523–5527, 1999.

Saiz-Lopez, A. and Boxe, C. S.: A mechanism for biologically-induced iodine emissions from sea-ice, Atmos. Chem. Phys. Discuss., 8, 2953–2976, doi:10.5194/acpd-8-2953-2008, 2008.

Saiz-Lopez, A., Mahajan, A. S., Salmon, R. A., Bauguitte, S. J.-B., Jones, A. E., Roscoe, H. K., and Plane, J. M. C.: Boundary layer halogens in coastal Antarctica, Science, 317, 348–351, 2007a.

Saiz-Lopez, A., Chance, K., Liu, X., Kurosu, T. P., and Sander, S. P.: First observations of iodine oxide from space, Geophys. Res. Lett., 34, L12812, doi:10.1029/2007GL030111, 2007b

Saiz-Lopez, A., Plane, J. M. C., Mahajan, A. S., Anderson, P. S., Bauguitte, S. J.-B., Jones, A. E., Roscoe, H. K., Salmon, R. A., Bloss, W. J., Lee, J. D., and Heard, D. E.: On the vertical distribution of boundary layer halogens over coastal Antarctica: implications for O3, HOx, NOx and the Hg lifetime, Atmos. Chem. Phys., 8, 887–900, doi:10.5194/acp-8-887-2008, 2008.

Salmon, R. A., Bauguitte, S. J.-B., Bloss, W., Hutterli, M. A., Jones, A. E., Read, K., and Wolff, E. W.: Measurement and interpretation of gas phase formaldehyde concentrations obtained during the CHABLIS campaign in coastal Antarctica, Atmos. Chem. Phys., 8, 4085–4093, doi:10.5194/acp-8-4085-2008, 2008.

Sander, S. P., Friedl, R. R., Golden, D. M., Kurylo, M. J., Moortgat, G. K., Keller-Rudek, H., Wine, P. H., Ravishankara, A. R., Kolb, C. E., Molina, M. J., Finlayson-Pitts, B. J., Huie, R. E., and Orkin, V. L.: Chemical Kinetics and Photochemical Data for Use in Atmospheric Studies – Evaluation Number 15, NASA-JPL Publication 06-2, Jet Propulsion Laboratory, California Institute of Technology, Pasadena, CA, 2006.

Saunders, R. W. and Plane, J. M. C.: Formation Pathways and Composition of Iodine Oxide Ultra-Fine Particles, Environ. Chem., 2, 299–303, 2005.

Schlosser, E., Brauers, T., Dorn, H.-P., Fuchs, H., Häseler, R., Hofzumahaus, A., Holland, F., Wahner, A., Kanaya, Y., Kajii, Y., Miyamoto, K., Nishida, S., Watanabe, K., Yoshino, A., Kubistin, D., Martinez, M., Rudolf, M., Harder, H., Berresheim, H., Elste, T., Plass-Dlmer, C., Stange, G., and Schurath, U.: Technical

Note: Formal blind intercomparison of OH measurements: results from the international campaign HOxComp, Atmos. Chem. Phys., 9, 7923–7948, doi:10.5194/acp-9-7923-2009, 2009.

Schönhardt, A., Richter, A., Wittrock, F., Kirk, H., Oetjen, H., Roscoe, H. K., and Burrows, J. P.: Observations of iodine monoxide columns from satellite, Atmos. Chem. Phys., 8, 637–653, doi:10.5194/acp-8-637-2008, 2008.

Shirley, T. R., Brune, W. H., Ren, X., Mao, J., Lesher, R., Cardenas, B., Volkamer, R., Molina, L. T., Molina, M. J., Lamb, B., Velasco, E., Jobson, T., and Alexander, M.: Atmospheric oxidation in the Mexico City Metropolitan Area (MCMA) during April 2003, Atmos. Chem. Phys., 6, 2753–2765, doi:10.5194/acp-6-2753-2006, 2006.

Simpson, W. R., von Glasow, R., Riedel, K., Anderson, P., Ariya, P., Bottenheim, J., Burrows, J., Carpenter, L. J., Frie, U., Goodsite, M. E., Heard, D., Hutterli, M., Jacobi, H.-W., Kaleschke, L., Neff, B., Plane, J., Platt, U., Richter, A., Roscoe, H., Sander, R., Shepson, P., Sodeau, J., Steffen, A., Wagner, T., and Wolff, E.: Halogens and their role in polar boundary-layer ozone depletion, Atmos. Chem. Phys., 7, 4375–4418, doi:10.5194/acp-7-4375-2007, 2007.

Sjostedt, S. J., Huey, L. G., Tanner, D. J., Peischl, J., Chen, G., Dibb, J. E., Lefer, B., Hutterli, M. A., Beyersdorf, A. J., Blake, N. J., Blake, D. R., Sueper, D., Ryerson, T., Burkhart, J., and Stohl, A.: Observations of hydroxyl and the sum of peroxy radicals at Summit, Greenland during summer 2003, Atm. Environ., 41, 5122–5137, 2007.

Sommariva, R., Bloss, W. J., Brough, N., Carslaw, N., Flynn, M., Haggerstone, A.-L., Heard, D. E., Hopkins, J. R., Lee, J. D., Lewis, A. C., McFiggans, G., Monks, P. S., Penkett, S. A., Pilling, M. J., Plane, J. M. C., Read, K. A., Saiz-Lopez, A., Rickard, A. R., and Williams, P. I.: OH and HO2 chemistry during NAMBLEX: roles of oxygenates, halogen oxides and heterogeneous uptake, Atmos. Chem. Phys., 6, 1135–1153, doi:10.5194/acp-6-1135-2006, 2006.

Sumner, A.-L., and Shepson, P. B.: Snowpack production of formaldehyde and its effect on the Arctic troposphere, Nature, 398, 230–233, 1999.

Tan. D., Faloona, I., Simpas, J. B., Brune, W., Olson, J., Crawford, J., Avery, M., Sachse, G., Vay, S., Sandholm, S., Guan, H.-W., Vaughn, T., Mastromarino, J., Heikes, B., Snow, J., Podolske, J., and Singh, H.: OH and HO2 in the tropical Pacific: Results from PEM-Tropics B, J. Geophys. Res., 106, 32667–32681, 2001.

Tucceri, M. E., Hölscher, D., Rodriguez, A., Dillon, T. J., and Crowley, J. N.: Absorption cross section and photolysis of OIO, Phys. Chem. Chem. Phys. 8, 834–846, 2006.

Wagenbach, D., Ducroz, F., Mulvaney, R., Keck, L., Minikin, A., LeGrand, M., Hall, J. S., and Wolff, E. W.: Sea-salt aerosol in coastal Antarctic regions, J. Geophys. Res. 103, 10961–10974, 1998.

Wolff, E. W.: Nitrate in Polar Ice, in: Ice core studies of global biogeochemical cycles, edited by: Delmas, R. J., Springer-Verlag, Berlin, Germany, 195–224, 1995.

Van den Bergh, H. and Troe, J.: Kinetic and thermodynamic properties of INO and INO2 intermediate complexes in iodine recombination, J. Chem. Phys., 64, 736–742, 1976.

Vogt, R., Sander, R., von Glasow, R., and Crutzen, P. J.: Iodine Chemistry and its Role in Halogen Activation and Ozone Loss in the Marine Boundary Layer: A Model Study, J. Atmos. Chem., 32, 375–395, 1999.

von Glasow, R. and Crutzen, P. J.: Tropospheric Halogen Chemistry, Treatise on Geochemistry, 4, 1–67, 2007.

Wang, Y., Choi, Y., Zeng, T., Davis, D., Buhr, M., Huey, L. G., and Neff, W.: Assessing the photochemical impact of snow NO_x emissions over Antarctica during ANTCI 2003, Atmos. Environ., 42, 2849–2863, 2008.

Zhou, X., Beine, H., Honrath, R. E., Fuentes, J. D., Simpson, W., Shepson, P. B., and Bottenheim, J. W.: Snowpack Photochemical Production of HONO: a Major source of OH in the Arctic Boundary Layer in Springtime, Geophys. Res. Lett., 28, 4087–4090, 2001.